This manuscript is the accepted version of the paper:

Pullout behaviour of geosynthetics in a recycled construction and demolition material - Effects of cyclic loading, Transportation Geotechnics, Vol. 23, Article number 100346, https://doi.org/10.1016/j.trgeo.2020.100346

Pullout behaviour of geosynthetics in a recycled construction and demolition material - Effects of cyclic loading

Castorina S. Vieira[1]*, Fernanda B. Ferreira[2], Paulo M. Pereira[3] and Maria de Lurdes Lopes[4]

[1]CONSTRUCT-Geo, University of Porto, Faculty of Engineering, R. Dr. Roberto Frias, 4200-465 Porto, Portugal, E-mail: cvieira@fe.up.pt

* Corresponding author

[2]CONSTRUCT-Geo, University of Porto, Faculty of Engineering, R. Dr. Roberto Frias, 4200-465 Porto, Portugal, E-mail: fbf@fe.up.pt

[3]CONSTRUCT-Geo, University of Porto, Faculty of Engineering, R. Dr. Roberto Frias, 4200-465 Porto, Portugal, E-mail: pmpp@fe.up.pt

[4]CONSTRUCT-Geo, University of Porto, Faculty of Engineering, R. Dr. Roberto Frias, 4200-465 Porto, Portugal, E-mail: lcosta@fe.up.pt

This manuscript is the accepted version of the paper:

Pullout behaviour of geosynthetics in a recycled construction and demolition material - Effects of cyclic loading, Transportation Geotechnics, Vol. 23, Article number 100346, https://doi.org/10.1016/j.trgeo.2020.100346

Pullout behaviour of geosynthetics in a recycled construction and demolition material - Effects of cyclic loading

Abstract

In recent years, the use of construction and demolition (C&D) materials as alternative aggregates in geotechnical engineering applications, such as embankments, pavement subbase layers and geosynthetic-reinforced structures has raised increasing attention from researchers and practitioners worldwide. On the other hand, geosynthetics, particularly geogrids and high strength geotextiles, are used as a reinforcement material in some of those applications. When these infrastructures are subjected to repeated loadings (e.g. traffic, wave and seismic loads), the understanding of the interaction properties at the backfill-geosynthetic interfaces under cyclic loading conditions is of primary interest. This paper describes an experimental study carried out using a large-scale pullout test apparatus to assess the load-strain-displacement behaviour of two geosynthetics embedded in a recycled C&D material under cyclic and post-cyclic loading conditions. Test results show that cyclic loading can measurably reduce the post-cyclic pullout resistance of the geotextile (up to 15%), when compared to that obtained from the benchmark monotonic test. Conversely, the cyclic loading did not significantly influence the pullout resistance of the geogrid. The cumulative cyclic displacements over the length of the geosynthetics were found to increase with the load amplitude and the pre-cyclic pullout load level. Moreover, under identical test conditions, the accumulated cyclic deformations along the geotextile length consistently exceeded those for the geogrid, possibly due to the lower tensile stiffness of the geotextile at low strains.

Keywords: Recycled construction and demolition materials, Sustainability, Geosynthetics, Cyclic loading, Pullout tests

This manuscript is the accepted version of the paper:

Pullout behaviour of geosynthetics in a recycled construction and demolition material - Effects of cyclic loading, Transportation Geotechnics, Vol. 23, Article number 100346, https://doi.org/10.1016/j.trgeo.2020.100346

1 INTRODUCTION

In recent years, waste generation and its efficient management has been pointed out as a key area of concern within the civil engineering industry at international level. Each year, billions of tons of construction and demolition (C&D) materials are produced globally from a range of activities, including excavation, site preparation, construction, maintenance and demolition of buildings and other civil infrastructures. This evidence, associated with the fact that the construction sector accounts for about 50% of all the materials extracted from the earth's crust [1] has intensified the pressure on the construction industry to develop and implement sustainable and economical waste recycling and valorisation strategies [2]. In this context, the use of recycled C&D wastes as an alternative to natural materials in civil engineering applications has been increasingly recognised as a potential means of addressing the environmental concerns arising from the scarcity of natural resources, as well as the large volumes of waste disposal to landfill. In particular, several studies have recently been conducted to assess the feasibility of using recycled C&D materials as alternative soils or aggregates in various geotechnical engineering works, such as road construction [3-11], ground improvement works [12-15], pipe bedding and backfilling [16, 17] and construction of geosynthetic-reinforced structures [18-20]. Although most of these studies have yielded encouraging results, suggesting that properly selected C&D materials may exhibit engineering properties equivalent or superior to those of typical quarry products, the recycling rates of C&D wastes in many countries, including Portugal, are still far below the target levels for satisfactory sustainable practice.

The application of geosynthetics, such as geogrids and geotextiles as reinforcement in geotechnical and transportation engineering projects, including retaining walls, road and railway embankments, steep slopes and bridge abutments to enhance the mechanical behaviour of soil has gained increasing acceptance worldwide. Among the main reasons for the popularity of these reinforced structures are the high cost-effectiveness, simple construction, ductility and flexibility, possibility to use lower quality backfill materials and satisfactory performance even when constructed in seismic areas.

For the safe design and adequate performance of geosynthetic-reinforced structures throughout their design working life, the geosynthetic tensile strength and the interaction characteristics at the interfaces between the geosynthetics and the backfill material should be properly understood. It should be noted that the pullout mechanism of a geotextile is different from that of a geogrid reinforcement. For geotextiles (with continuous surface), only the frictional resistance contributes to the overall pullout resistance. However, for geogrids, the pullout capacity results from the skin friction on the surface of the geogrid longitudinal and transverse members (i.e. frictional resistance) and the bearing resistance mobilised against the transverse members (passive resistance). Regardless of the reinforcement type, a condition for verification of internal stability is that the tensile force acting on the reinforcement should not exceed its pullout strength in the anchorage zone (beyond the hypothetical failure surface). The pullout resistance of geosynthetics in the anchorage zone of geosynthetic-reinforced structures is therefore required by design codes for stability analysis [21-24].

The soil-geosynthetic interface behaviour has been extensively investigated over the past decades using different test methods, such as the direct shear test [25-30], pullout test [31-35], inclined plane test [36-39] and in-soil tensile test [40]. However, only limited effort has been expended to characterise the interaction between geosynthetics and recycled C&D materials [41-44, 19, 45].

Touahamia et al. [38] carried out a series of large-scale direct shear tests on unreinforced and geogrid-reinforced recycled construction materials, such as crushed concrete and building debris. Although the angles of internal friction of the recycled materials were found to be lower than that of a freshly quarried basalt aggregate, the presence of the geogrid reinforcement led to a significant increase in the shearing resistance of these recycled materials, while also greatly restraining the deformation of the specimens.

To ascertain the potential use of recycled C&D wastes as backfill of reinforced soil structures, Santos and Vilar [36] evaluated the geotechnical and chemical properties of a recycled C&D aggregate, as well as the interface behaviour between the recycled material and a geogrid under pullout loading conditions. The internal friction angle of the C&D aggregate ($\phi = 42°$) was greater than that of the reference material used by the authors (a standard sand complying with the specifications of the FHWA for backfill materials of reinforced soil structures, with $\phi = 32°$). Moreover, the results of the pullout tests showed that the C&D material-geogrid interfaces yielded better performance than those involving the standard sand.

Arulrajah et al. [43] investigated the interface shear strength properties of various C&D aggregates (i.e. recycled concrete aggregate, crushed brick and reclaimed asphalt pavement) reinforced with biaxial and triaxial geogrids, using a modified large-scale direct shear test apparatus. The interface peak shear strength properties of the recycled concrete aggregate were consistently higher than those for the other recycled materials. The geogrid-reinforced C&D materials were found to meet the peak and residual shear strength requirements for construction aggregates typically used in civil engineering applications.

More recently, Vieira and Pereira [37, 39] examined the direct shear behaviour of different geosynthetic-C&D material interfaces under various conditions of moisture content and density using a large-scale direct shear test apparatus. The coefficients of interaction obtained for the studied interfaces (0.61-0.94) compared well with those generally found in the literature for soil-geosynthetic interfaces. Additionally, the authors evaluated the pullout behaviour of different geosynthetics embedded in a recycled C&D material, using a large-scale pullout test device [19]. The results from the pullout tests also supported the feasibility of using these recycled C&D wastes as alternative backfill materials for reinforced soil construction.

In addition to static loads, geosynthetic-reinforced structures built with recycled C&D materials may also be subjected to repeated loads, such as those generated by traffic and earthquakes, in which case the understanding of the fill material-geosynthetic interaction under cyclic loading conditions is essential [46, 47, 28, 48-52]. While some studies have been conducted on C&D materials under repeated load triaxial testing [53-55], to the best of the authors' knowledge, no previous studies have been reported on the interface strength properties of geosynthetic-reinforced C&D materials under repeated loadings. In this present study, a large-scale pullout test apparatus was used to investigate the behaviour of two different geosynthetics (a uniaxial geocomposite reinforcement, or high-strength geotextile, and an extruded uniaxial geogrid) embedded in a recycled C&D material and subjected to monotonic and cyclic pullout loads. A series of monotonic and multistage pullout tests (consisting of monotonic, cyclic and post-cyclic phases) was conducted, with the goal being to examine the effect of the pre-cyclic pullout load level (i.e. static pullout force at the start of the cyclic phase), frequency and amplitude of the sinusoidal cyclic load and geosynthetic type on the load-strain-displacement behaviour of the reinforcements. Furthermore, to determine whether the imposed cyclic loading has the potential to detrimentally affect the pullout resistance of the geosynthetics, a comparison is made between the maximum pullout forces reached in the post-cyclic phase of the multistage tests and those attained in monotonic tests carried out under otherwise identical test conditions.

2 EXPERIMENTAL STUDY

2.1 Recycled C&D material

The fine-grained recycled C&D material used in this study was collected from a recycling plant located in central Portugal and derived mainly from the demolition of house buildings and cleaning of lands with illegal dumps of C&D wastes. It should be noted that this C&D material resulted from a recycling process, in which any unwanted materials (such as plastics, cork, steel, wood, rubbers, paper and cardboard, textiles, foams, among others) were removed, the materials were crushed and then subjected to grain-size separation. To ascertain the compatibility of this material with the relevant standards, a comprehensive physical, mechanical and environmental characterisation was carried out prior to the actual pullout testing. The constituents of the C&D material were evaluated by hand sorting of particles, following the European Standard EN 933-11:2009 [56], with a slight modification related to the non-inclusion of soils in the “other materials” category. As shown in **Table 1**, the material consisted mainly of concrete and mortar products, unbound aggregates, masonries and soil.

The particle size distribution (PSD) of the C&D material was determined by sieving and sedimentation, following the EN 933-1:2012 [57] and CEN ISO/TS 17892-4:2004 [58] standards, respectively. **Fig. 1** compares the PSD of this recycled material with the gradation limits specified by the Federal Highway Administration, FHWA [23] and the National Concrete Masonry Association, NCMA [21] for backfill materials of mechanically stabilised earth walls

(MSEW), reinforced soil slopes (RSS) and segmental retaining walls (SRW). It can be concluded that the material fulfils the gradation requirements of the FHWA for reinforced soil slopes and of the NCMA for segmental retaining walls, although not complying with the recommendations of the FHWA for mechanically stabilised earth walls.

The physical and geotechnical properties of the recycled C&D material are listed in **Table 2**. The quality of fines was assessed through the methylene blue test, according to the European Standard EN 933-9:2009 [59]. The value of the methylene blue (MB) expressed in grams of dye per kilogram of the 0-2 mm size fraction was 3.2 g/kg. The dry density-moisture content relationship was evaluated using the Modified Proctor test, following EN 13286-2:2002 [60]. From this test, the maximum dry density ($\gamma_{d,max}$ = 20.1 kN/m^3) and optimum moisture content (w_{opt} = 9%) were obtained. Furthermore, the breakage of the C&D material after the Modified Proctor test was evaluated by comparing the particle size distribution curves before and after the test. The particle breakage was found to be almost negligible.

The internal shear strength of the C&D material when compacted to the dry unit weight (γ_d) of 16.1 kN/m^3 (corresponding to 80% of its maximum dry density) and at the optimum moisture content (according to the Modified Proctor test [60]) was estimated using a large-scale direct shear box (300 mm wide × 600 mm long × 200 mm deep). The direct shear tests were carried out under the normal stresses of 25, 50, 100 and 150 kPa. **Fig. 2** shows the values of peak shear stress plotted against the normal stress, as well as the corresponding best-fit straight line. Based on the Mohr-Coulomb failure criterion, the shear strength of this C&D material can be characterised by a friction angle (ϕ) of 37.6° and cohesion (c) of 16.3 kPa.

The content of water soluble sulphates in aggregates is an important parameter that needs to be controlled and kept below a certain level, since sulfate contaminants may give rise to expansive disruption of concrete. In the specific case of recycled C&D materials to be used as backfill of geosynthetic-reinforced structures, this parameter needs to be controlled since the aggregates might be in contact with concrete elements, such as concrete facing elements, bridge foundations, among others. The content of water soluble sulphates of the C&D material used in this study was estimated by spectrophotometry, as per Section 10 of the EN 1744-

1:2009 [61]. First, specimens of the C&D material were sieved through a 4 mm sieve and the retained particles were crushed to pass the same sieve. The specimens were then mixed with hot water to extract water-soluble sulphate ions. Barium chloride was added so that sulphate ions precipitate as barium sulphate. The mean value of the water soluble sulphates obtained by weighting and expressed as a percentage of sulphate ions by mass of tested material was 0.14%.

The use of alternative backfill materials may raise environmental concerns related to the contamination of the ground water. To assess the potential short-term release of dangerous substances, laboratory leaching tests were carried out on the recycled C&D material, following the EN 12457-4:2002 [62]. **Table 3** presents the results of the laboratory leaching tests, along with the acceptance criteria of maximum leached concentration for inert landfill, as established by the European Council Decision 2003/33/EC [63]. It can be concluded that only the sulphate content exceeds the limit specified by the European legislation for inert materials. The Federal Highway Administration recommends the use of backfill materials with a pH value ranging from 5 to 10 for the construction of mechanically stabilized earth walls and reinforced soil slopes [23]. As shown in **Table 3**, the pH value of this C&D material (pH = 8.2) is within the FHWA recommended range.

2.2 Geosynthetics

Two commercially available geosynthetics commonly used for soil reinforcement were tested (**Fig. 3**): a uniaxial geocomposite reinforcement (GCR), also referred to as a high-strength geotextile, consisting of high strength polyester (PET) fibres attached to a continuous filament nonwoven polypropylene (PP) geotextile, and an extruded uniaxial high-density polyethylene (HDPE) geogrid (GGR). The in-isolation tensile strength of the geosynthetics was evaluated by laboratory tensile tests performed according to ISO 10319:2015 [64]. The tensile load-strain curves for five specimens of each geosynthetic tested under repeatability conditions, as well as the corresponding mean curves are presented in **Fig. 4**. **Table 4** summarises the main physical and mechanical properties of these materials.

2.3 Apparatus and test procedures

Fig. 5a shows an overall view of the pullout test apparatus used in this current study. The equipment is composed of a large pullout box (1.53 m long, 1.00 m wide and 0.80 m deep), a vertical load application system, a horizontal force actuator device and all the required instrumentation (i.e., displacement transducers, load cells and linear potentiometers). To minimise the frictional effects of the front wall boundary, the apparatus is equipped with a 0.20 m long sleeve.

The recycled C&D material was compacted inside the pullout box in four 0.15 m thick layers, using an electric vibratory hammer, so as to achieve the target dry unit weight of 16.1 kN/m^3 (corresponding to 80% of the maximum Modified Proctor dry density) at the optimum moisture content (w_{opt} = 9%). Once the two initial layers were placed and compacted, the geosynthetic specimen (with initial dimensions of 0.25 m wide × 0.75 m long or 0.20 m wide × 0.60 m long, for the geotextile and the geogrid, respectively) was clamped and laid over the C&D material. To monitor the displacements along the length of the specimen, a set of inextensible wires were attached to the geosynthetic, at one end, and to linear potentiometers located at the back of the pullout box, at the opposite end (**Figs. 5b** and **5c**). The remaining two layers of filling material were then placed and compacted, resulting in a total height of 0.60 m. The vertical pressure on the top layer of C&D material was applied through a wooden plate, which was loaded by ten hydraulic jacks, and its magnitude was controlled by a load cell. To attenuate the top boundary-fill friction and obtain more uniform distribution of the vertical stresses, a neoprene slab was installed between the loading plate and the top layer of fill material.

The pullout load was applied to the geosynthetic specimen through a hydraulic system and the geosynthetic front displacement (i.e. clamp displacement) was recorded by a linear potentiometer. The multistage tests were carried out under load-controlled conditions and consisted of three successive stages. In the first stage, a constant load increment rate of 0.2 kN/min was applied until a pre-established value of the pullout force (referred to in this paper as the pre-cyclic pullout load level, P_L) was reached. In the next stage (cyclic loading phase), a sinusoidal cyclic pullout force of constant frequency (f) and amplitude (A) was imposed for 100 cycles. After that, the test was again carried out under constant load increment rate (0.2 kN/min), until the pullout or tensile failure of the reinforcement was detected. In order to analyse the potential effect of cyclic loading on the pullout resistance of the geosynthetics, a comparison was made between the maximum pullout forces recorded in the third phase of the multistage tests and those from benchmark monotonic tests performed under load-controlled conditions (i.e. under a constant load increment rate of 0.2 kN/min).

During the tests, the pullout force, front displacement of the geosynthetic specimen, displacements over the length of the reinforcement and the applied normal stress were continuously monitored. Further details on the pullout test apparatus and test procedures can be found in Ferreira et al. [34].

2.4 Test programme

Table 5 summarises the test conditions adopted in the pullout tests T1 to T13 carried out in the present research. To evaluate the influence of the pre-cyclic pullout load level (i.e. pullout force reached when the cyclic stage starts) on the pullout behaviour of the geosynthetics, different P_L values specified as a function of the pullout resistance (P_R) attained under monotonic loading conditions were considered: $P_L = 0.40\ P_R$ and $0.70\ P_R$. These P_L values were selected in order to simulate two different levels of static pullout force already acting on the reinforcement when the cyclic loading is applied. In geosynthetic-reinforced soil systems, geosynthetics may be subjected to different static tensile forces, due to the self-weight of the structure and eventual external dead loads. These two P_L values aimed at simulating a relatively low and a high static pullout force acting on the reinforcement, for comparison purposes. The influence of the loading frequency was assessed by applying sinusoidal waves with frequencies of 0.05 Hz and 0.1 Hz. The amplitude of the cyclic load was also defined as a function of P_R and varied between $0.20\ P_R$ and $0.40\ P_R$. A fixed number of load cycles, n, equal to 100 was applied in the multistage tests. Monotonic load-controlled pullout tests were also conducted on both geosynthetics and used as a benchmark for assessing the effect of cyclic loading on the pullout response of the geosynthetics. In order to simulate low depths, where the pullout failure is most likely to occur in geosynthetic-reinforced structures, all the tests were conducted under a low vertical pressure, σ_v (25 kPa at the interface level).

3 RESULTS AND DISCUSSION

3.1 Effect of the pre-cyclic pullout load level

As mentioned previously, to investigate the influence of the pre-cyclic pullout load level on the pullout response of the geosynthetics, different values of P_L were imposed (0.4 P_R and 0.7 P_R). **Fig. 6a** compares the evolution of the pullout force with the front displacement obtained from multistage test T1, which was carried out on the geotextile under $P_L = 0.4\ P_R$, f = 0.1 Hz and A = 0.2 P_R, with that from the benchmark monotonic test (test T12). The total displacements (i.e. resulting from sliding and elongation) measured along the length of the reinforcement during the cyclic stage are presented in **Fig. 6b**. Similarly, **Figs. 6c** and **6d** present the results obtained when the highest value of P_L was considered (test T5). It can be concluded that, regardless of the value of P_L, the cyclic loading led to a decrease in the maximum pullout force recorded in the tests, with respect to that achieved in the comparable monotonic test. This reduction was particularly significant under $P_L = 0.7\ P_R$ (15.4%), when compared to the lower reduction of 7.3% corresponding to $P_L = 0.4\ P_R$.

The evolution of the pullout force with the front displacement for the benchmark monotonic test (test T12) shows a decrease in the interface stiffness occurring around $0.55P_L$. This evidence has significant influence on the interface behaviour above this level. Fig. 6c reveals that when the highest value of P_L was imposed to the interface, the above-mentioned drop point had already been exceeded and the interface was unable to provide suitable pullout strength to respond to the imposed load.

Fig. 6 also shows that the failure mode when the interface is subjected to previous cyclic loading differed from that observed under monotonic loading conditions. Indeed, while in the monotonic test the failure was caused by a lack of tensile strength of the reinforcement (tensile failure), suggesting that the pullout resistance exceeded the tensile strength of the geosynthetic under these confinement conditions, in the multistage tests the failure was caused by sliding of the specimen along the interface (pullout failure). The change of failure mode (from tensile to pullout failure) when the interface is previously subjected to cyclic loading may be associated with the cyclic load-induced deformations along the length of the reinforcement and progressive mobilisation of sections towards the reinforcement free end, which promotes the pullout trigger condition (i.e. when the rear end of the reinforcement begins to move) and associated pullout failure during the post-cyclic stage of the multistage tests.

As expected, the displacements measured over the geosynthetic length at the start of the cyclic loading phase (i.e. for n = 0) increased with the pre-cyclic pullout load level (**Figs. 6b** and **6d**). **Fig. 6b** indicates that, for $P_L = 0.4\ P_R$, the displacements/deformations along the geotextile resulting from cyclic loading were generally negligible, except for the section adjacent to the clamp system, which experienced increasing deformation throughout the load cycles. However, in test T5 involving a higher P_L value, the displacements/deformations along the geosynthetic length increased significantly with the number of cycles (**Fig. 6d**). This is possibly associated with the fact that the full geosynthetic length had already been mobilised when the cyclic stage started, as indicated by the displacement profile corresponding to n = 0. Similar conclusions were also drawn from the comparison of the results obtained under different P_L values when a lower frequency of 0.5 Hz was adopted (tests T3 and T7). These observations suggest that the pre-cyclic pullout load level has the potential to greatly affect the incremental displacements measured along the length of the geotextile during cyclic loading, as well as the pullout resistance of the reinforcement after cyclic loading.

Fig. 7 illustrates the influence of P_L on the cumulative displacements recorded during the load cycles at the front and rear ends of the geotextile in tests performed under different values of load frequency and amplitude. Regardless of the frequency (i.e. 0.1 or 0.05 Hz) and amplitude (i.e. 0.2 or 0.4 P_R), the accumulated front displacements of the geotextile increased with the number of cycles and reached significantly larger values under the highest P_L. In general, higher increments of front displacement were obtained during the initial stage of cyclic loading, with a gradually decreasing trend being observed during subsequent cycling (**Figs. 7a**, **7c** and **7e**). On the other hand, the accumulated displacements at the rear end of the specimens were practically unnoticeable (**Figs. 7b**, **7d** and **7f**). It is noteworthy that in the test conducted simultaneously under the highest values of P_L and A (i.e. $P_L = 0.7\ P_R$ and $A = 0.4\ P_R$ – test T6), the cyclic loading induced the failure of the interface (after about 40 cycles), which prevented the completion of the pre-established number of cycles (**Fig. 7c**).

The effect of P_L on the pullout response of the geogrid when subjected to a cyclic loading with frequency of 0.1 Hz and amplitude equal to 0.2 P_R is shown in **Fig. 8** (tests T8 and T10). The results indicate that the maximum pullout forces reached in the tests were not significantly affected by the applied cyclic loadings (**Figs. 8a** and **8c**). However, for $P_L = 0.7\ P_R$, the failure occurred by sliding of the geogrid along the interface, unlike the tensile failure observed in the monotonic test. This finding suggests that cyclic loading for high levels of tensile force installed in the geogrid may change the pullout behaviour of the geogrid, such that it can induce the pullout failure of the reinforcement in situations where the failure would otherwise be determined by a lack of tensile strength.

As shown in **Figs. 8b** and **8d**, the displacements recorded along the length of the geogrid specimens during cyclic loading increased progressively with the load cycles and were more pronounced under the highest P_L value, corroborating the results obtained for the geotextile. The influence of P_L on the geogrid deformation behaviour during cyclic loading is further clarified in **Fig. 9**, which plots the accumulated displacements at the front and rear ends of the geogrid specimens under different values of load amplitude. The incremental displacements were particularly significant during the initial load cycles, with a decreasing rate being observed subsequently. Furthermore, the cumulative displacements at either end of the reinforcement were consistently larger under $P_L = 0.7\ P_R$. For instance, upon the application of 100 load cycles with amplitude of 0.4 P_R, the cumulative front displacement of the geogrid reached about 20 mm for $P_L = 0.4\ P_R$, whereas it exceeded 40 mm for $P_L = 0.7\ P_R$ (**Fig. 9c**). This value exceeds the limit value of 30 mm beyond which a medium height geosynthetic-reinforced wall constructed with a granular backfill can be considered to be performing poorly or be potentially unstable [65].

3.2 Effect of the load frequency

The effect of the cyclic load frequency on the pullout behaviour of the geotextile was evaluated by comparing the results from multistage tests carried out at the frequencies of 0.1 and 0.05 Hz. **Fig. 10** presents the results obtained under $P_L = 0.4\ P_R$, $A = 0.2\ P_R$ and different frequencies (tests T1 and T3), whereas **Fig. 11** shows the experimental data corresponding to $P_L = 0.4\ P_R$ and a higher value of the load amplitude, $A = 0.4\ P_R$ (tests T2 and T4). **Figs. 10a** and **10c** suggest that the cyclic load frequency may affect the maximum pullout force as well as the failure mode observed during the post-cyclic stage of the test. In fact, when the test was carried out under 0.1 Hz frequency loading (**Fig. 10a**), the failure was caused by sliding of the reinforcement along the interface and the maximum pullout force was about 7.3% lower than that obtained under monotonic loading conditions. However, under 0.05 Hz frequency loading (**Fig. 10c**), the failure resulted from insufficient tensile strength of the reinforcement and the maximum pullout force was close to that attained in the monotonic test.

For these specific test conditions ($P_L = 0.4\ P_R$ and $A = 0.2\ P_R$), the displacements recorded along the geosynthetic length during the cyclic phase were not significantly influenced by the load frequency and only the first instrumented section (i.e. front section) contributed to the mobilisation of pullout forces (**Figs. 10b** and **10d**). However, under a higher amplitude loading ($A = 0.4\ P_R$), the effect of frequency on the displacements measured over the reinforcement length appear to be more pronounced (**Figs. 11b** and **11d**), with the higher frequency loading inducing greater deformations along the length of the specimen.

As shown in **Figs. 11a** and **11c**, when the loading rate decreased from 0.1 to 0.05 Hz, the interface failure mode changed from pullout to tensile failure, corroborating the results obtained under the lower amplitude of 0.2 P_R. As noted earlier, for the multistage test in which the failure occurred due to a lack of tensile strength of the reinforcement, the cyclic loading had little effect on the maximum pullout force reached in the test (**Fig. 11c**).

Fig. 12 compares the accumulated displacements recorded at the front and rear ends of the geotextile specimens during cyclic loading when the frequencies of 0.1 and 0.05 Hz were imposed. With regard to the displacements measured at the front end of the geosynthetic, the results did not show any clear trend. On the other hand, the displacements measured at the rear end of the reinforcement were negligible regardless of frequency, which means that no sliding occurred during the cyclic stage of these tests. Moraci and Cardile [47] studied the effect of the cyclic load frequency on the deformation behaviour of different geogrids embedded in a compacted uniform sand when subjected to cyclic pullout forces with frequencies of 0.05 and 0.1 Hz. The authors reported that, for the test conditions investigated, the effect of frequency on the accumulated displacements and deformations along the specimens was almost negligible. The influence of the load frequency on the pullout response of an extruded uniaxial geogrid embedded in a well-graded residual soil was also investigated in a previous study by Ferreira et. al. [52], whereby the accumulated displacements over the length of the reinforcement were observed to decrease progressively with increasing frequency (from 0.01 to 1 Hz). These findings suggest that the effect of frequency on the pullout behaviour of embedded geosynthetics may be dependent upon the backfill and geosynthetic types, as well as the characteristics of the applied cyclic loading, and hence further studies would be useful to get further insight into this interdependency.

3.3 Effect of the load amplitude

The effect of the load amplitude on the pullout behavior of the geotextile can be analysed comparing **Fig. 6a** and **Fig. 6b** with the results plotted in **Fig. 11a** and **Fig. 11b**, relating to tests T1 and T2, respectively. In these tests the geotextile was subjected to a cyclic loading starting at $P_L = 0.4\ P_R$, with the frequency of 0.1 Hz and different amplitudes ($A = 0.2\ P_R$ and $0.4\ P_R$). As mentioned before and irrespective of the amplitude value, the cyclic loading led to a reduction in the maximum pullout force reached in the tests.

Comparing the graphs plotted in **Fig. 6b** and **Fig. 11b** it can be noted that the deformation behaviour of the reinforcement during cyclic loading was highly influenced by the load amplitude. In fact, while for $A = 0.2\ P_R$ (**Fig. 6b**) only the section of the geosynthetic adjacent to the clamp experienced deformation, under the higher amplitude of $0.4\ P_R$ (**Fig. 11b**) most of the reinforcement length was mobilised. Therefore, the increase in amplitude not only induced substantially greater incremental deformations at the front section of the reinforcement, but also led to the mobilisation of sections located towards its opposite (free) end. The rear segment, however, did not experience any significant deformation, regardless of the load amplitude.

The influence of the load amplitude on the accumulated displacements at the front and rear ends of the geotextile under different values of P_L and frequency is shown in **Fig. 13**. It can clearly be seen that the displacements recorded at the front end of the geosynthetic increased substantially with the load amplitude, regardless of P_L and frequency (**Figs. 13a**, **13c** and **13e**). While in the tests carried out under $P_L = 0.4\ P_R$ the cumulative front displacements tended to increase at a progressively decreasing rate during the cyclic process (for both values of amplitude), in the tests under $P_L = 0.7\ P_R$ the increase in amplitude from 0.2 to 0.4 P_R led to the rupture of the PET yarns, and hence to tensile failure of the geotextile during the cyclic phase. As mentioned, the cumulative displacements at the rear end of the specimens were negligible, indicating that no sliding occurred upon cyclic loading, regardless of the amplitude.

Fig. 14 demonstrates how the cyclic load amplitude affected the pullout response of the geogrid in tests performed under $P_L = 0.4\ P_R$ and f = 0.1 Hz (tests T8 and T9). For the tested conditions, the load amplitude does not seem to have a significant influence on the pullout resistance of the geogrid. The maximum pullout force attained in the multistage tests was comparable to that reached in the respective monotonic test (**Figs. 14a** and **14c**). However, the total displacements measured throughout the geogrid length during the cyclic stage were found to increase with the load amplitude (**Figs. 14b** and **14d**).

3.4 Effect of the geosynthetic type

The influence of the geosynthetic type on the pullout test results was investigated by comparing the load-strain-displacement behaviour of the geotextile and the geogrid in multistage tests performed under a constant frequency of 0.1 Hz and different amplitudes and pre-cyclic pullout load levels. The pullout force-front displacement curves from multistage tests T2 and T9 carried out on the different geosynthetics under $A = 0.4\ P_R$ and $P_L = 0.4\ P_R$ are depicted in **Figs. 15a** and **15c**, along with the corresponding monotonic curves. In turn, the displacement profiles along the length of the reinforcements are shown in **Figs. 15b** and **15d**. The results indicate that significantly larger front displacements were produced during the cyclic phase in the test involving the geotextile (**Fig. 15a**), when compared with those for the geogrid (**Fig. 15c**). When the geotextile was tested, the peak pullout force recorded in the third stage of the test (i.e. after cyclic loading) decreased about 12.7%, with respect to the value obtained under monotonic loading conditions. However, for the geogrid and as mentioned before, the peak pullout force remained nearly unchanged despite of cyclic loading. The displacements (and associated deformations) measured over the length of the geotextile during the cyclic phase clearly exceeded those of the geogrid, particularly in the sections closer to the point of load application (**Figs. 15b** and **15d**).

The pullout behaviour of the geosynthetics is further compared in **Fig. 16**, which shows the results from tests T6 and T11, performed under A = 0.4 P_R and P_L = 0.7 P_R. Under these specific test conditions, the geotextile failed during cyclic loading by insufficient tensile strength under confined conditions, upon the accumulation of large deformations at the front section (**Figs. 16a** and **16b**). As mentioned before, the evolution of the pullout force with the front displacement for the geotextile exhibits a slight breaking point for a tensile force around 0.55P_L (**Fig. 16a**). Consequently, when the cyclic loading phase starts at P_L = 0.7 P_R the interface is unable to provide suitable pullout strength to respond to the imposed load. In contrast, the geogrid failure occurred during the post-cyclic stage of the test and at a pullout force that was similar to that attained under monotonic conditions, thus exhibiting better performance than the geotextile under these loading conditions (**Figs. 16c** and **16d**).

The influence of the geosynthetic type on the accumulated displacements at the front and rear ends of the specimens during cyclic loading is illustrated in **Fig. 17**. Except for the tests carried out under the lowest values of P_L and A (P_L = 0.4 P_R and A = 0.2 P_R), in which the front and rear displacements for both geosynthetics were rather similar (**Figs. 17a** and **17b**), the accumulated displacements at the front end of the geotextile specimens were significantly higher than those for the geogrid (**Figs. 17c**, **17e** and **17g**). This is likely associated with the lower tensile stiffness of the geotextile at low strains (as observed in the in-isolation tensile tests). Conversely, the cumulative displacements measured at the rear end of the geogrid specimens were generally higher than those for the geotextile (**Figs. 17d**, **17f** and **17h**). However, once the passive resistance against the geogrid transverse bars was mobilised, only minor increments of rear displacement were subsequently obtained due to the contribution of the passive resistance mechanism to the overall pullout capacity of the geogrid.

3.5 Discussion

Table 6 summarises the values of the accumulated displacement at the front end (d_F) and at the rear end (d_R) of the geosynthetic specimens, the accumulated deformations at the front section of the specimens (ε_F) and the average accumulated deformations along the length of the reinforcements (ε_A) measured during the cyclic phase of the multistage tests T1 to T11.

The accumulated displacements at the front end of the geosynthetics ranged from 12.0 mm to 110.4 mm, with the highest value corresponding to test T6, in which the geotextile failure occurred during the cyclic loading stage. As expected, the accumulated displacements at the rear end of the specimens were substantially lower than those at the front end, due to the extensible nature of the geosynthetics and the development of progressive failure mechanisms at the reinforcement-backfill interface. It can also be observed that the accumulated deformations generated at the front section of the geosynthetics during cyclic loading (calculated for the frontal 150 mm and 130 mm in the geotextile and geogrid, respectively) ranged from 2.5% to 18.1%, whereas the average accumulated deformations ranged from 1.6% to 14.8%. In general, the deformations at the front section of the geosynthetics were larger than the average accumulated deformations along the full length of the reinforcements. Under identical test conditions, the accumulated cyclic deformations at the front section, as well as the average accumulated deformations throughout the length of the geotextile consistently exceeded those for the geogrid, which indicates the geogrid exhibited stiffer response under the applied cyclic loadings.

Table 7 presents the values of the maximum pullout force (P_R), the corresponding front displacement of the geosynthetic specimen (d_{PR}) and the interface failure mode observed in the monotonic and multistage pullout tests carried out in this study. Also shown in this table are the percent variations of P_R (ΔP_R) and d_{PR} (Δd_{PR}) for the multistage tests with respect to the values obtained in the respective monotonic test.

The results indicate that, for the geotextile, the application of cyclic loading led to important reductions (up to 15.4%) of the maximum pullout force, in comparison to that obtained in the monotonic test. Additionally, the front displacement at maximum pullout force generally increased with the presence of cyclic loading.

In the case of the geogrid, the influence of cyclic loading on the post-cyclic pullout resistance was almost negligible. In some of the multistage tests (tests T9 and T11), the pullout resistance even exceeded the value obtained under monotonic loading conditions, suggesting that cyclic loading may occasionally improve the interaction properties at the interface. The movement of the geogrid specimen during cyclic loading (i.e. back and forth movement) and the associated soil dragging led to the generation of lifts in front of the geogrid transverse members, particularly in the tests carried out under higher displacement amplitude (i.e. tests T9 and T11, performed under A = 0.4 P_R). This is turn contributed to the increase in the passive resistance mobilised against the transverse bars in the post-cyclic stage of the test, leading to stiffer post-cyclic interface response and greater pullout capacity.

Based on the above observations, it can be concluded that the geogrid exhibited better performance than the geotextile under the cyclic loading conditions investigated in this study.

4 CONCLUSIONS

This study investigated the pullout behaviour of two geosynthetics embedded in a compacted C&D recycled material through a series of monotonic and multistage pullout tests. Special emphasis was given to the effects of the pre-cyclic pullout load level, frequency and amplitude of the cyclic load and geosynthetic type on the cyclic and post-cyclic load-strain-displacement response of the reinforcements. The most relevant findings of the study are summarised below.

- The tensile strength of both geosynthetics under confined conditions (i.e, embedded in a recycled C&D material) is lower than that achieved in in-isolation tensile tests. It is important to point out that this evidence has also been observed when the geosynthetics are embedded in natural soils and it shows the importance of understanding the pullout behavior of the geosynthetics embedded in the filling material to be used in the construction of the structure or infrastructrure.

- Cyclic loading can measurably reduce the pullout resistance of the geotextile, comparatively with that attained under monotonic loading conditions (up to 15.4% in this study). The degradation of the pullout resistance became more pronounced as the pre-cyclic pullout load level, load frequency and amplitude were increased. However, for the geogrid, the effect of cyclic loading on the maximum pullout forces mobilised in the tests was almost negligible, having been achieved a slight increase in the pullout resistance in most cases.
- The interface failure mode of the geotextile changed from pullout to tensile failure when the loading frequency decreased from 0.1 to 0.05 Hz. Further studies would be useful to clarify the influence of the loading frequency on the pullout behaviour.
- In general, the displacements recorded along the length of the geosynthetics during the cyclic phase of the multistage tests increased with the number of cycles at a progressively decreasing rate. While for the geotextile the obtained displacements resulted mainly from the deformation of the specimens, for the geogrid the displacements derived from both deformation and sliding along the interface.
- The cumulative displacements measured over the length of the geosynthetics during cyclic loading increased significantly with the pre-cyclic pullout load level and the load amplitude.
- Under certain conditions, the application of cyclic loading may influence the interface failure mode in the post-cyclic stage of the tests, leading to the pullout failure of the geosynthetics, which would otherwise be determined by the lack of tensile strength of the reinforcements (as observed in the monotonic tests).

The results reported in this paper provide important insight into the performance of two geosynthetics commonly used in the construction of geosynthetic-reinforced structures when

This manuscript is the accepted version of the paper:

Pullout behaviour of geosynthetics in a recycled construction and demolition material - Effects of cyclic loading, Transportation Geotechnics, Vol. 23, Article number 100346, https://doi.org/10.1016/j.trgeo.2020.100346

embedded in a C&D recycled material and subjected to cyclic pullout loadings. Since the pullout resistance of the interface involving the high-strength geotextile was found to reduce upon cyclic loading, special care should be taken when defining the interface strength parameters used in the design of geosynthetic-reinforced structures under repeated loadings. When these parameters are estimated from monotonic testing, proper reduction factors should be considered to account for the potential degradation of the pullout resistance of the reinforcement in the presence of cyclic loading.

CREDIT AUTHORSHIP CONTRIBUTION STATEMENT

Castorina Vieira: Conceptualization; Funding acquisition; Methodology; Project administration; Writing – review & editing. Fernanda Ferreira: Methodology; Data curation; Formal analysis; Writing - original draft. Paulo Pereira: Methodology; Data curation. Maria de Lurdes Lopes: Conceptualization; Funding acquisition; Methodology.

DECLARATION OF COMPETING INTEREST

The authors declare that they have no known competing financial interests or personal relationships that could have appeared to influence the work reported in this paper.

ACKNOWLEDGMENTS

This work was financially supported by the Research Project CDW_LongTerm, POCI-01-0145-FEDER-030452, funded by FEDER funds through COMPETE2020 - Programa Operacional Competitividade e Internacionalização (POCI) and by national funds (PIDDAC) through FCT/MCTES.

REFERENCES

1. European Commission. Competitiveness of the Construction Industry. A Report drawn up by the Working Group for Sustainable Construction with participants from the European Commission, Member States and Industry. European Commission, Brussels, 2001.

2. D. Basu, A. Misra and A. J. Puppala, "Sustainability and geotechnical engineering: perspectives and review," *Canadian Geotechnical Journal*, vol. 52, no. 1, pp. 96-113, 2014.

3. C. S. Poon and D. Chan, "Feasible use of recycled concrete aggregates and crushed clay brick as unbound road sub-base," *Construction and Building Materials*, vol. 20, no. 8, pp. 578-585, 2006.

4. F. D. Leite, R. D. Motta, K. L. Vasconcelos and L. Bernucci, "Laboratory evaluation of recycled construction and demolition waste for pavements," *Construction and Building Materials*, vol. 25, no. 6, pp. 2972-2979, 2011.

5. A. Arulrajah, J. Piratheepan, M. W. Bo and N. Sivakugan, "Geotechnical characteristics of recycled crushed brick blends for pavement sub-base applications," *Canadian Geotechnical*, vol. 49, no. 7, pp. 796-811, 2012.

6. A. Barbudo, F. Agrela, J. Ayuso, J. R. Jiménez and C. S. Poon, "Statistical analysis of recycled aggregates derived from different sources for sub-base applications," *Construction and Building Materials*, vol. 28, no. 1, pp. 129-138, 2012.

7. J. R. Jiménez, J. Ayuso, A. P. Galvín, M. López and F. Agrela, "Use of mixed recycled aggregates with a low embodied energy from non-selected CDW in unpaved rural roads," *Construction and Building Materials*, vol. 34, pp. 34-43, 2012.

8. A. Arulrajah, J. Piratheepan, M. M. Disfani and M. W. Bo, "Geotechnical and geoenvironmental properties of recycled construction and demolition materials in pavement subbase applications," *Journal of Materials in Civil Engineering*, vol. 25, no. 8, pp. 1077-1088, 2013.

9. I. Del Rey, J. Ayuso, A. P. Galvín, J. R. Jiménez and A. Barbudo, "Feasibility of using unbound mixed recycled aggregates from CDW over expansive clay subgrade in unpaved rural roads," *Materials*, vol. 9, no. 11, Article number 931, 2016.

10. M. Aboutalebi Esfahani, "Evaluating the feasibility, usability, and strength of recycled construction and demolition waste in base and subbase courses," *Road Materials and Pavement Design*, vol. 21, no. 1, pp. 156-178, 2018.

11. A. R. Pasandín and I. Pérez, "Performance of hot-mix asphalt involving recycled concrete aggregates," *International Journal of Pavement Engineering* 2018 (In press).

12. A. Kumar Suluguru, M. Jayatheja, A. Kar, A. GuhaRay, S. R. Surana and N. James, "Experimental studies on the microstructural, physical and chemical characteristics of building derived materials to assess their suitability in ground improvement," *Construction and Building Materials*, vol. 156, pp. 921-932, 2017.

13. N. Cristelo, A. Fernández-Jiménez, C. Vieira, T. Miranda and Á. Palomo, "Stabilisation of construction and demolition waste with a high fines content using alkali activated fly ash," *Construction and Building Materials*, vol. 170, pp. 26-39, 2018.

14. C. Henzinger and D. Heyer, "Soil improvement using recycled aggregates from demolition waste," *Proceedings of the Institution of Civil Engineers: Ground Improvement*, vol. 171, no. 2, pp. 74-81, 2018.

15. M. Kianimehr, P. T. Shourijeh, S. M. Binesh, A. Mohammadinia and A. Arulrajah, "Utilization of recycled concrete aggregates for light-stabilization of clay soils," *Construction and Building Materials*, vol. 227, pp. 116792, 2019.

16. M. A. Rahman, M. Imteaz, A. Arulrajah and M. M. Disfani, "Suitability of recycled construction and demolition aggregates as alternative pipe backfilling materials," *Journal of Cleaner Production*, vol. 66, pp. 75-84, 2014.

17. C. S. Vieira, M. L. Lopes and N. Cristelo. Geotechnical characterization of recycled C&D wastes for use as trenches backfilling. Proceedings of the International Conference WASTES: Solutions, Treatments and Opportunities, pp. 175-182, 2018.

18. E. C. G. Santos, E. M. Palmeira and R. J. Bathurst, "Behaviour of a geogrid reinforced wall built with recycled construction and demolition waste backfill on a collapsible foundation," *Geotextiles and Geomembranes*, vol. 39, pp. 9-19, 2013.

19. C. S. Vieira, P. M. Pereira and M. L. Lopes, "Recycled construction and demolition wastes as filling material for geosynthetic reinforced structures. Interface properties," *Journal of Cleaner Production*, vol. 124, pp. 299-311, 2016.

20. C. S. Vieira, "Valorization of Fine-Grain Construction and Demolition (C&D) Waste in Geosynthetic Reinforced Structures," *Waste and Biomass Valorization*, DOI: 10.1007/s12649-018-0480-x, 2018 (In press).

21. NCMA. Design manual for segmental retaining walls (2nd ed.), National Concrete Masonry Association (ed. J. Collin), Herndon, VA, USA, 1997.

22. Canadian Geotechnical Society. Canadian Foundation Engineering Manual, 4th ed., BiTech Publisher Ltd., Richmond, BC, Canada, 2006.

23. FHWA. Design of mechanically stabilized earth walls and reinforced soil slopes – Volume I, FHWA-NHI-10-024 (editors Berg, R.R., Christopher, B.R., Samtani, N.C.), Federal Highway Administration, Washington, D.C., 2009.

24. AASHTO. LRFD Bridge Design Specifications. 8th edition, American Association of State Highway and Transportation Officials, Washington, D.C., USA, 2017.

25. M. Abu-Farsakh, J. Coronel and M. Tao, "Effect of soil moisture content and dry density on cohesive soil–geosynthetic interactions using large direct shear tests," *Journal of Materials in Civil Engineering*, vol. 19, no. 7, pp. 540-549, 2007.

26. C.-N. Liu, Y.-H. Ho and J.-W. Huang, "Large scale direct shear tests of soil/PET-yarn geogrid interfaces," *Geotextiles and Geomembranes*, vol. 27, no. 1, pp. 19-30, 2009.

27. F. B. Ferreira, C. S. Vieira and M. L. Lopes. Analysis of soil-geosynthetic interfaces shear strength through direct shear tests. Proceedings of the International Symposium on Design and Practice of Geosynthetic-Reinforced Soil Structures, pp. 44-53, 2013.

28. C. S. Vieira, M. L. Lopes and L. M. Caldeira, "Sand–geotextile interface characterisation through monotonic and cyclic direct shear tests," *Geosynthetics International*, vol. 20, no. 1, pp. 26-38, 2013.

29. D. Esmaili, K. Hatami and G. A. Miller, "Influence of matric suction on geotextile reinforcement-marginal soil interface strength," *Geotextiles and Geomembranes*, vol. 42, no. 2, pp. 139-153, 2014.

30. F. B. Ferreira, C. S. Vieira and M. L. Lopes, "Direct shear behaviour of residual soil–geosynthetic interfaces – influence of soil moisture content, soil density and geosynthetic type," *Geosynthetics International*, vol. 2, no. 3, pp. 257 –272, 2015.

31. M. L. Lopes and M. Ladeira, "Influence of the confinement, soil density and displacement rate on soil-geogrid interaction," *Geotextiles and Geomembranes*, vol. 14, no. 10, pp. 543-554, 1996.

32. E. M. Palmeira, "Bearing force mobilisation in pull-out tests on geogrids," *Geotextiles and Geomembranes*, vol. 22, no. 6, pp. 481-509, 2004.

33. N. Moraci and P. Recalcati, "Factors affecting the pullout behaviour of extruded geogrids embedded in a compacted granular soil," *Geotextiles and Geomembranes*, vol. 24, no. 4, pp. 220-242, 2006.

34. F. B. Ferreira, C. S. Vieira, M. L. Lopes and D. M. Carlos, "Experimental investigation on the pullout behaviour of geosynthetics embedded in a granite residual soil," *European Journal of Environmental and Civil Engineering*, vol. 20, no. 9, pp. 1147-1180, 2016.

35. F. B. Ferreira, C. S. Vieira and M. L. Lopes, "Pullout behaviour of different geosynthetics - influence of soil density and moisture content," *Frontiers in Built Environment*, DOI: 10.3389/fbuil.2020.00012, 2020 (Ahead of print).

36. H. N. Pitanga, J. P. Gourc and O. M. Vilar, "Interface shear strength of geosynthetics: Evaluation and analysis of inclined plane tests," *Geotextiles and Geomembranes*, vol. 27, no. 6, pp. 435-446, 2009.

37. L. Briançon, H. Girard and J. P. Gourc, "A new procedure for measuring geosynthetic friction with an inclined plane," *Geotextiles and Geomembranes*, vol. 29, pp. 472-482, 2011.

38. M. L. Lopes, F. B. Ferreira, J. R. Carneiro and C. S. Vieira, "Soil-geosynthetic inclined plane shear behavior: influence of soil moisture content and geosynthetic type," *International Journal of Geotechnical Engineering*, vol. 8, no. 3, pp. 335-342, 2014.

39. F. B. Ferreira, C. S. Vieira and M. L. Lopes. Soil-geosynthetic interface strength properties from inclined plane and direct shear tests - A comparative analysis. Proceedings of GA 2016 - 6th Asian Regional Conference on Geosynthetics: Geosynthetics for Infrastructure Development, pp. 925-937, 2016.

40. M. J. Mendes, E. M. Palmeira and E. Matheus, "Some factors affecting the in-soil load-strain behaviour of virgin and damaged nonwoven geotextiles," *Geosynthetics International*, vol. 14, no. 1, pp. 39-50, 2007.

41. M. Touahamia, V. Sivakumar and D. McKelvey, "Shear strength of reinforced-recycled material," *Construction and Building Materials*, vol. 16, no. 6, pp. 331-339, 2002.

42. E. C. G. Santos and O. M. Vilar. Use of Recycled Construction and Demolition Wastes (RCDW) as Backfill of Reinforced Soil Structures. Proceedings of the 4th European Geosynthetics Conference, EUROGEO 4; Edimburg, 7-10 September 2008, Paper N.º 199, 2008.

43. A. Arulrajah, M. A. Rahman, J. Piratheepan, M. W. Bo and M. A. Imteaz, "Evaluation of Interface Shear Strength Properties of Geogrid-Reinforced Construction and Demolition Materials using a Modified Large Scale Direct Shear Testing Apparatus," *Journal of Materials in Civil Engineering*, vol. 26, no. 5, pp. 974-982, 2014.

44. C. S. Vieira and P. M. Pereira, "Interface shear properties of geosynthetics and construction and demolition waste from large-scale direct shear tests," *Geosynthetics International*, vol. 23, no. 1, pp. 62-70, 2016.

45. C. S. Vieira and P. M. Pereira, "Use of mixed construction and demolition recycled materials in geosynthetic reinforced embankments," *Indian Geotechnical Journal*, vol. 48, no. 2, pp. 279-292, 2018.

46. N. Moraci and G. Cardile, "Influence of cyclic tensile loading on pullout resistance of geogrids embedded in a compacted granular soil," *Geotextiles and Geomembranes*, vol. 27, no. 6, pp. 475-487, 2009.

47. N. Moraci and G. Cardile, "Deformative behaviour of different geogrids embedded in a granular soil under monotonic and cyclic pullout loads," *Geotextiles and Geomembranes*, vol. 32, pp. 104-110, 2012.

48. F. B. Ferreira, C. S. Vieira and M. L. Lopes. Cyclic and post-cyclic shear behaviour of a granite residual soil-geogrid interface. Procedia Engineering, Vol 143, Advances in Transportation Geotechnics III, pp. 379-386, 2016.

49. F. Y. Liu, P. Wang, X. Geng, J. Wang and X. Lin, "Cyclic and post-cyclic behaviour from sand–geogrid interface large-scale direct shear tests," *Geosynthetics International*, vol. 23, no. 2, pp. 129-139, 2016.

50. J. Wang, F. Y. Liu, P. Wang and Y. Q. Cai, "Particle size effects on coarse soil-geogrid interface response in cyclic and post-cyclic direct shear tests," *Geotextiles and Geomembranes*, vol. 44, no. 6, pp. 854-861, 2016.

51. G. Cardile, M. Pisano and N. Moraci, "The influence of a cyclic loading history on soil-geogrid interaction under pullout condition," *Geotextiles and Geomembranes*, vol. 47, no. 4, pp. 552-565, 2019.

52. F. B. Ferreira, C. S. Vieira, M. L. Lopes and P. G. Ferreira, "HDPE geogrid-residual soil interaction under monotonic and cyclic pullout loading," *Geosynthetics International*, DOI: 10.1680/jgein.19.00057, 2020 (Ahead of Print).

53. A. Arulrajah, J. Piratheepan, T. Aatheesan and M. W. Bo, "Geotechnical Properties of Recycled Crushed Brick in Pavement Applications," *Journal of Materials in Civil Engineering*, vol. 23, no. 10, pp. 1444-1452, 2011.

54. A. Arulrajah, E. Yaghoubi, Y. C. Wong and S. Horpibulsuk, "Recycled plastic granules and demolition wastes as construction materials: Resilient moduli and strength characteristics," *Construction and Building Materials*, vol. 147, pp. 639-647, 2017.

55. A. Arulrajah, M. Naeini, A. Mohammadinia, S. Horpibulsuk and M. Leong, "Recovered plastic and demolition waste blends as railway capping materials," *Transportation Geotechnics*, vol. 22, Article number 100320, 2020.

56. EN 933-11:2009. Tests for geometrical properties of aggregates – Part 11: Classification test for the constituents of coarse recycled aggregate. CEN, 2009.

57. EN 933-1:2012. Tests for geometrical properties of aggregates – Part 1: Determination of particle size distribution – Sieving method. CEN, 2012.

58. CEN ISO/TS 17892-4:2004. Geotechnical investigation and testing - laboratory testing of soil - Part 4: Determination of particle size distribution. CEN (in collaboration with ISO), 2004.

59. EN 933-9:2009. Tests for geometrical properties of aggregates. Assessment of fines. Methylene blue test. CEN, 2009.

60. EN 13286-2:2002. Unbound and hydraulically bound mixtures - Part 2: Test methods for laboratory reference density and water content - Proctor compaction. CEN, 2002.

61. EN 1744-1:2009. Tests for chemical properties of aggregates - Part 1: Chemical analysis. CEN, 2009.

62. EN 12457-4:2002. Characterisation of waste – Leaching – Compliance test for leaching of granular waste material and sludges – Part 4. CEN, 2002.

63. EC, "Council Decision 2003/33/EC establishing criteria and procedures for the acceptance of waste at landfills pursuant to Article 16 of and Annex II to Directive 1999/31/EC," *Official Journal of the European Union*, vol. L11/27, 2003.

64. ISO 10319. Geosynthetics - Wide-width tensile test. International Organization for Standardization, 2015.

65. T. M. Allen and R. J. Bathurst, "Observed long-term performance of geosynthetic walls and implications for design," *Geosynthetics International*, vol. 9, no. 5-6, pp. 567-606, 2002.

66. BS 1377-2. Methods of test for soils for civil engineering purposes. Classification tests. British Standard Institution, 1990.

67. ASTM D 4253. Standard test methods for maximum index density and unit weight of soils using a vibratory table. American Society for Testing and Materials, 2006.

68. ASTM D 4254. Standard test methods for minimum index density and unit weight of soils and calculation of relative density. American Society for Testing and Materials, 2006.

This manuscript is the accepted version of the paper:

Pullout behaviour of geosynthetics in a recycled construction and demolition material - Effects of cyclic loading, Transportation Geotechnics, Vol. 23, Article number 100346, https://doi.org/10.1016/j.trgeo.2020.100346

LIST OF SYMBOLS

A – cyclic load amplitude (N/m)

c – cohesion of the fill material (Pa)

D_x – diameter corresponding to x% passing of the fill material (m)

e_{max} – maximum void ratio (dimensionless)

e_{min} – minimum void ratio (dimensionless)

f – cyclic load frequency (Hz)

G – specific gravity of particles (dimensionless)

L_R - confined length of the reinforcement at maximum pullout force (m)

MB - Methylene blue value (dimensionless)

n – number of load cycles (dimensionless)

P_L – pullout load level at the start of the cyclic loading phase (N/m)

P_R – pullout resistance per unit width of reinforcement (N/m)

d_{PR} – front displacement of the reinforcement at maximum pullout force (m)

d_F – accumulated displacement at the front end of the reinforcement (m)

d_R – accumulated displacement at the rear end of the reinforcement (m)

w_{opt} – optimum moisture content (dimensionless)

γ_d – dry unit weight (N/m^3)

$\gamma_{d,\ max}$ – maximum dry unit weight (N/m^3)

ΔP_R – percent variation of P_R with respect to the value obtained under monotonic loading conditions (dimensionless)

Δd_{PR} – percent variation of d_{PR} with respect to the value obtained under monotonic conditions (dimensionless)

ε_F – accumulated deformation at the front section of the geogrid (dimensionless)

ε_A – average accumulated deformation over the length of the geogrid (dimensionless)

ϕ – internal friction angle of the fill material (degrees)

This manuscript is the accepted version of the paper:

Pullout behaviour of geosynthetics in a recycled construction and demolition material - Effects of cyclic loading, Transportation Geotechnics, Vol. 23, Article number 100346, https://doi.org/10.1016/j.trgeo.2020.100346

LIST OF TABLES

LIST OF FIGURES

Fig. 11. Effect of frequency on the pullout behaviour of the GCR (P_L = 0.4 P_R, A = 0.4 P_R): (a) pullout force vs front displacement (f = 0.1 Hz); (b) total displacement over the GCR length (f = 0.1 Hz); (c) pullout force vs front displacement (f = 0.05 Hz); (d) total displacement over the GCR length (f = 0.05 Hz).

Fig. 12. Effect of frequency on the displacements accumulated at the GCR ends during cyclic loading: (a) front end (tests T1 and T3); (b) rear end (tests T1 and T3); (c) front end (tests T2 and T4); (d) rear end (tests T2 and T4); (e) front end (tests T5 and T7); (f) rear end (tests T5 and T7).

Fig. 13. Effect of amplitude on the displacements accumulated at the GCR ends during cyclic loading: (a) front end (tests T1 and T2); (b) rear end (tests T1 and T2); (c) front end (tests T3 and T4); (d) rear end (tests T3 and T4); (e) front end (tests T5 and T6); (f) rear end (tests T5 and T6).

Fig. 14. Effect of amplitude on the pullout behaviour of the GGR (P_L = 0.4 P_R, f = 0.1 Hz): (a) pullout force vs front displacement (A = 0.2 P_R); (b) total displacement over the GGR length (A = 0.2 P_R); (c) pullout force vs front displacement (A = 0.4 P_R); (d) total displacement over the GGR length (A = 0.4 P_R).

Fig. 15. Effect of geosynthetic type for P_L = 0.4 P_R, f = 0.1 Hz and A = 0.4 P_R: (a) pullout force vs front displacement of the GCR; (b) total displacement over the GCR length; (c) pullout force vs front displacement of the GGR; (d) total displacement over the GGR length.

Fig. 16. Effect of geosynthetic type for P_L = 0.7 P_R, f = 0.1 Hz and A = 0.4 P_R: (a) pullout force vs front displacement of the GCR; (b) total displacement over the GCR length; (c) pullout force vs front displacement of the GGR; (d) total displacement over the GGR length.

Fig. 17. Effect of geosynthetic type on the displacements accumulated at the reinforcement ends during cyclic loading: (a) front end (tests T1 and T8); (b) rear end (tests T1 and T8); (c) front end (tests T2 and T9); (d) rear end (tests T2 and T9); (e) front end (tests T5 and T10); (f) rear end (tests T5 and T10); (g) front end (tests T6 and T11); (h) rear end (tests T6 and T11).

This manuscript is the accepted version of the paper:

Pullout behaviour of geosynthetics in a recycled construction and demolition material - Effects of cyclic loading, Transportation Geotechnics, Vol. 23, Article number 100346, https://doi.org/10.1016/j.trgeo.2020.100346

Table 1. Proportion of constituents of the recycled C&D material.

Constituents (EN 933-11 [56])	
Concrete products, concrete and mortar (%)	40.0
Unbound aggregates, natural stone, aggregates treated with hydraulic binders (%)	36.5
Masonry units of clay materials, masonry units of calcium silicate and aerated non-floating concrete (%)	10.8
Bituminous materials (%)	0.5
Glass (%)	1.2
Soils (%)	10.8
Other materials: rubber, metals, non-floating wood, plaster,… (%)	0.1
Floating particles (cm^3/kg)	10.0

This manuscript is the accepted version of the paper:

Pullout behaviour of geosynthetics in a recycled construction and demolition material - Effects of cyclic loading, Transportation Geotechnics, Vol. 23, Article number 100346, https://doi.org/10.1016/j.trgeo.2020.100346

Table 2. Physical and geotechnical properties of the recycled C&D material.

Properties	Test method	Value
D_{10} (mm)	CEN ISO/TS 17892-4 [58]	0.01
D_{50} (mm)	CEN ISO/TS 17892-4 [58]	0.65
D_{60} (mm)	CEN ISO/TS 17892-4 [58]	1.03
Particles density, G_s	BS 1377-2 [66]	2.58
Minimum void ratio, e_{min}	ASTM D 4253 [67]	0.434
Maximum void ratio, e_{max}	ASTM D 4254 [68]	0.877
Methylene blue value, MB (g/kg)	EN 933-9 [59]	3.2
Maximum dry density, $\gamma_{d,max}$ (kN/m^3)	EN 13286-2 [60]	20.1
Optimum water content, w_{opt} (%)	EN 13286-2 [60]	9.0

Note: D_{10}, D_{50} and D_{60} are characteristic grain diameters

Table 3. Results of laboratory leaching tests of the recycled C&D material.

Parameter	Value (mg/kg)	Acceptance criteria – Inert landfill (mg/kg)
Arsenic, As	0.021	0.5
Lead, Pb	<0.01	0.5
Cadmium, Cd	<0.003	0.04
Chromium, Cr	0.012	0.5
Copper, Cu	0.10	2
Nickel, Ni	0.011	0.4
Mercury, Hg	<0.002	0.01
Zinc, Zn	<0.1	4
Barium, Ba	0.11	20
Molybdenum, Mo	0.018	0.5
Antimony, Sb	<0.01	0.06
Selenium, Se	<0.02	0.1
Chloride, Cl	300	800
Fluoride, F	6.1	10
Sulphate, SO4	3200	1000
Phenol index	<0.05	1
Dissolved Organic Carbon, DOC	220	500
pH	8.2	-

Table 4. Physical and mechanical properties of the geosynthetics.

	GCR	GGR
Raw material	PP & PET	HDPE
Mass per unit area (g/m^2)	340	450
Aperture dimensions (mm)	-	16 × 219
With of longitudinal members (mm)	-	6
With of transverse members (mm)	-	16
Thickness of longitudinal members (mm)	-	1.1
Thickness of transverse members (mm)	-	2.5 to 2.7
Mean value of the tensile strength***** (kN/m)	75	68
Mean value of the tensile strength† (kN/m)	70.6	60.3
Elongation at maximum load***** (%)	10	11 ± 3
Elongation at maximum load† (%)	9.7	10.1
Secant stiffness at 5% strain† (kN/m)	573.1	718.0

***** Values provided by the manufacturers (machine direction)

† Values obtained from laboratory tensile tests as per ISO 10319 [64] (machine direction)

Table 5. Test programme.

Test	Test type	Geosynthetic	P_L	f (Hz)	A	n	σ_v (kPa)
T1	Multistage	GCR	0.4 P_R	0.1	0.2 P_R	100	25
T2	Multistage	GCR	0.4 P_R	0.1	0.4 P_R	100	25
T3	Multistage	GCR	0.4 P_R	0.05	0.2 P_R	100	25
T4	Multistage	GCR	0.4 P_R	0.05	0.4 P_R	100	25
T5	Multistage	GCR	0.7 P_R	0.1	0.2 P_R	100	25
T6	Multistage	GCR	0.7 P_R	0.1	0.4 P_R	100	25
T7	Multistage	GCR	0.7 P_R	0.05	0.2 P_R	100	25
T8	Multistage	GGR	0.4 P_R	0.1	0.2 P_R	100	25
T9	Multistage	GGR	0.4 P_R	0.1	0.4 P_R	100	25
T10	Multistage	GGR	0.7 P_R	0.1	0.2 P_R	100	25
T11	Multistage	GGR	0.7 P_R	0.1	0.4 P_R	100	25
T12	Monotonic	GCR	-	-	-	-	25
T13	Monotonic	GGR	-	-	-	-	25

Table 6. Accumulated displacements and deformations of the geosynthetics during cyclic loading.

	Test	d_F (mm)	d_R (mm)	ε_F* (%)	ε_A (%)
Geotextile (GCR)	T1	12.32	0	5.23	1.89
	T2	70.07	0.07	18.13	10.64
	T3	13.6	0	5.29	2.09
	T4	49.85	0	11.68	7.62
	T5	50.57	2.89	4.24	6.56
	T6	110.35	3.85	16.70	14.76
	T7	73.53	1.31	7.80	10.31
Geogrid (GGR)	T8	11.97	2.28	2.46	1.57
	T9	19.81	6.79	2.49	2.11
	T10	27.03	11.62	3.35	2.43
	T11	43.76	16.08	2.89	4.35

***** Calculated for the frontal 150 mm and 130 mm in the geotextile and geogrid, respectively.

Table 7. Pullout resistance and failure mode of the geosynthetics.

	Test	P_L	f (Hz)	A	P_R (kN/m)	d_{PR} (mm)	Failure mode	ΔP_R (%)	Δd_{PR} (%)
Geotextile (GCR)	T1	0.4 P_R	0.1	0.2 P_R	56.79	203.91	Pullout	-7.31	10.13
	T2	0.4 P_R	0.1	0.4 P_R	53.51	209.68	Pullout	-12.66	13.25
	T3	0.4 P_R	0.05	0.2 P_R	60.54	159.59	Tensile	-1.18	-13.81
	T4	0.4 P_R	0.05	0.4 P_R	57.29	186.89	Tensile	-6.49	0.94
	T5	0.7 P_R	0.1	0.2 P_R	51.83	191.13	Pullout	-15.40	3.23
	T6*	0.7 P_R	0.1	0.4 P_R	-	-	Pullout/Tensile	-	-
	T7	0.7 P_R	0.05	0.2 P_R	52.80	200.1	Pullout	-13.83	8.07
Geogrid (GGR)	T8	0.4 P_R	0.1	0.2 P_R	49.25	101.19	Tensile	-1.87	-8.75
	T9	0.4 P_R	0.1	0.4 P_R	51.67	100.71	Tensile	2.96	-9.18
	T10	0.7 P_R	0.1	0.2 P_R	49.91	131.54	Pullout	-0.55	18.62
	T11	0.7 P_R	0.1	0.4 P_R	52.57	115.45	Tensile	4.74	4.11
GCR	T12	-	-	-	61.27	185.15	Tensile	-	-
GGR	T13	-	-	-	50.19	110.89	Tensile	-	-

***** The failure occurred during the cyclic loading phase

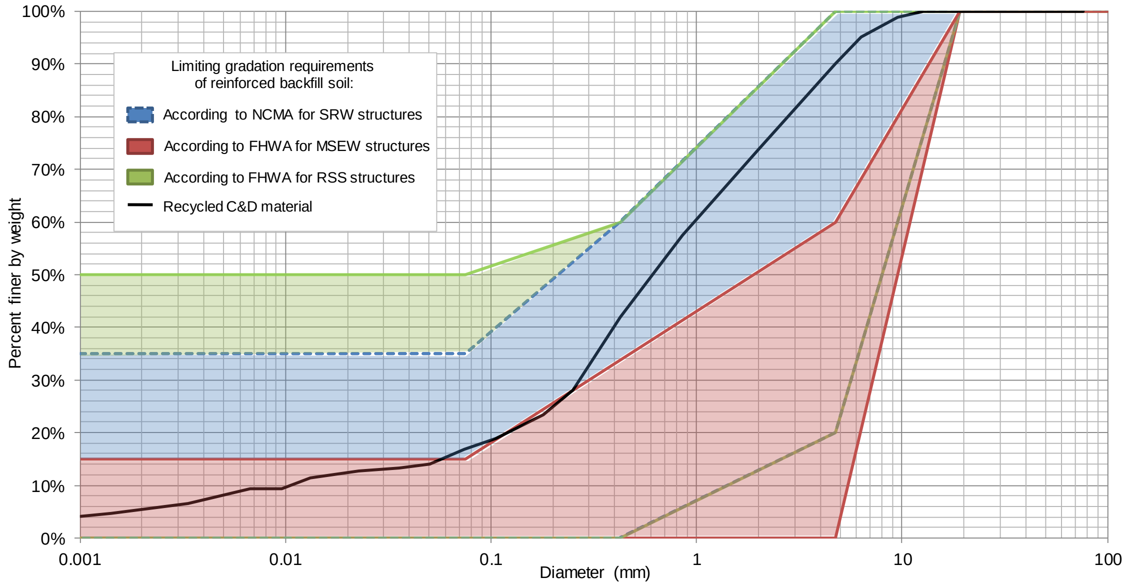

Fig. 1. Particle size distribution curve of the recycled C&D material and gradation limits recommended by FHWA and NCMA for reinforced soil construction.

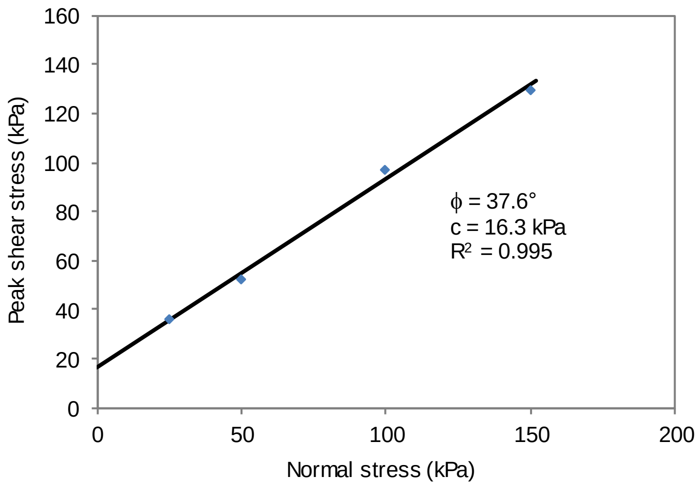

Fig. 2. Failure envelope and direct shear strength parameters of the recycled C&D material.

(a)

(b)

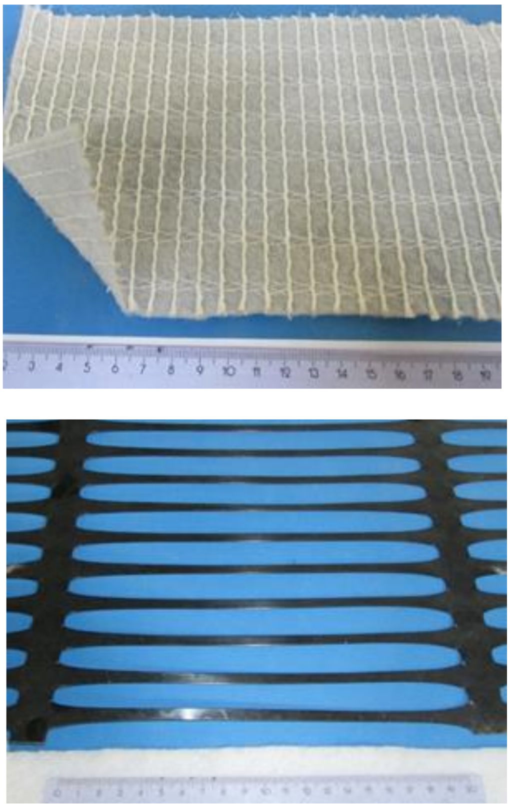

Fig. 3. Visual aspect of the geosynthetics (ruller in centimetres): (a) high-strength geotextile (GCR); (b) geogrid (GGR).

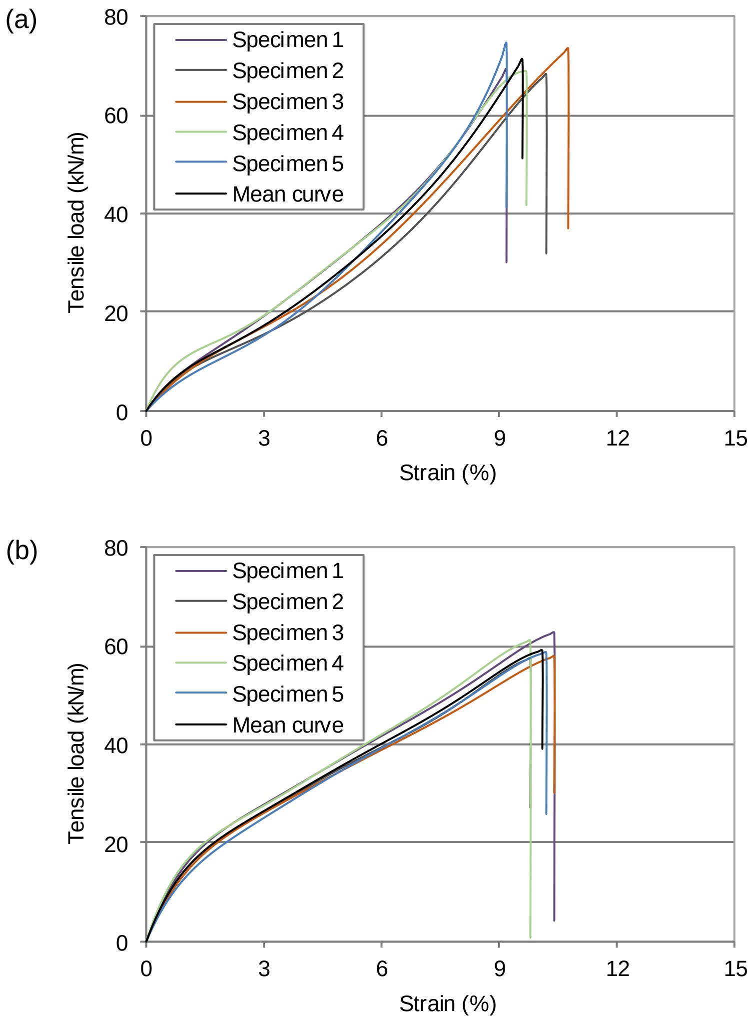

Fig. 4. Tensile load-strain curves of the geosynthetics in the machine direction: (a) geotextile (GCR); (b) geogrid (GGR).

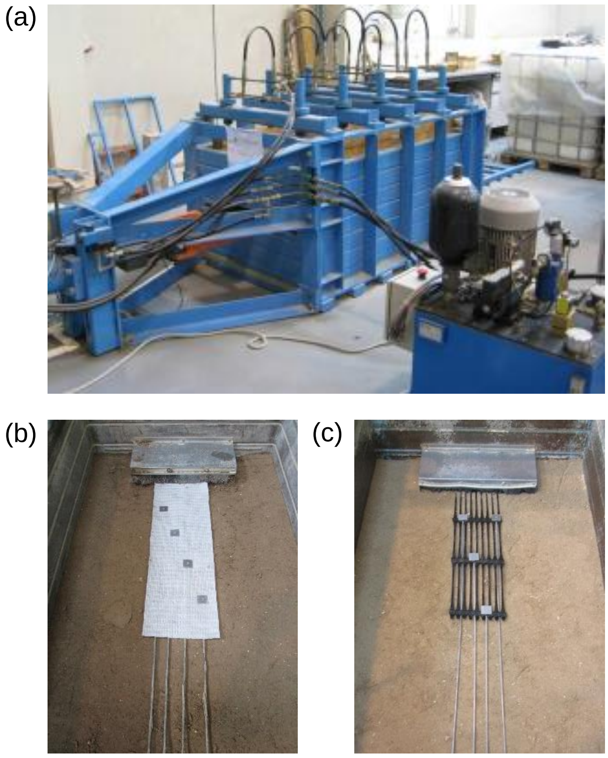

Fig. 5. Pullout test apparatus: (a) general overview; (b) inextensible wires connected to the geotextile specimen; (c) inextensible wires connected to the geogrid specimen.

This manuscript is the accepted version of the paper:

Pullout behaviour of geosynthetics in a recycled construction and demolition material - Effects of cyclic loading, Transportation Geotechnics, Vol. 23, Article number 100346, https://doi.org/10.1016/j.trgeo.2020.100346

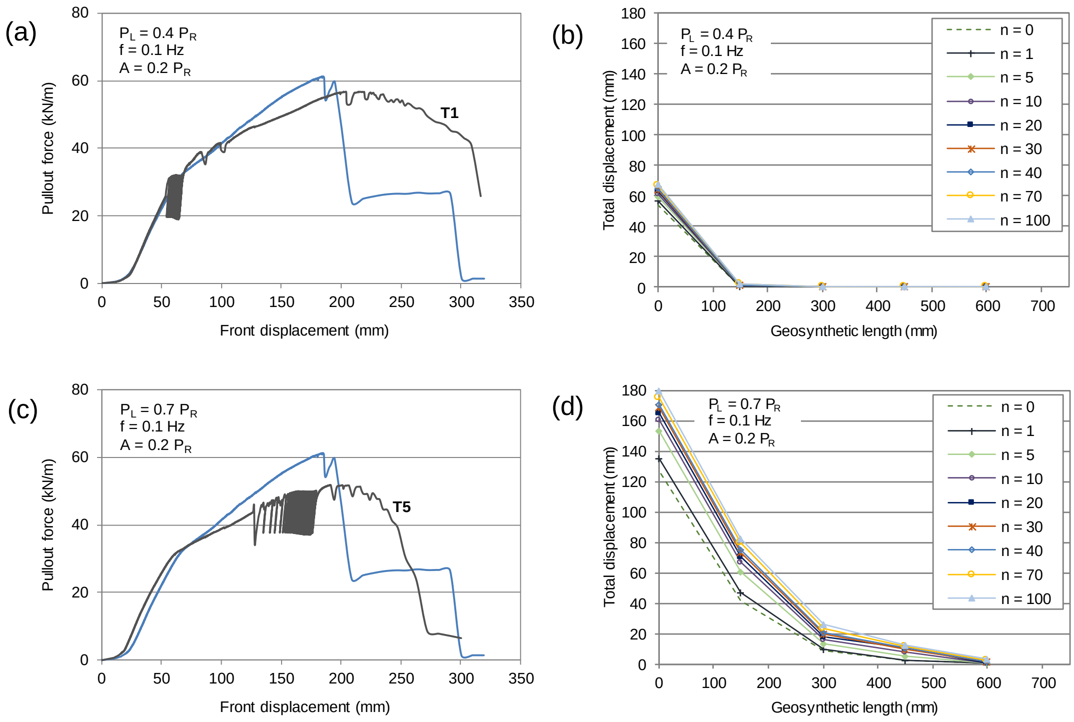

Fig. 6. Effect of P_L on the pullout behaviour of the GCR (f = 0.1 Hz, A = 0.2 P_R): (a) pullout force vs front displacement (P_L = 0.4 P_R); (b) total displacement over the GCR length (P_L = 0.4 P_R); (c) pullout force vs front displacement (P_L = 0.7 P_R); (d) total displacement over the GCR length (P_L = 0.7 P_R).

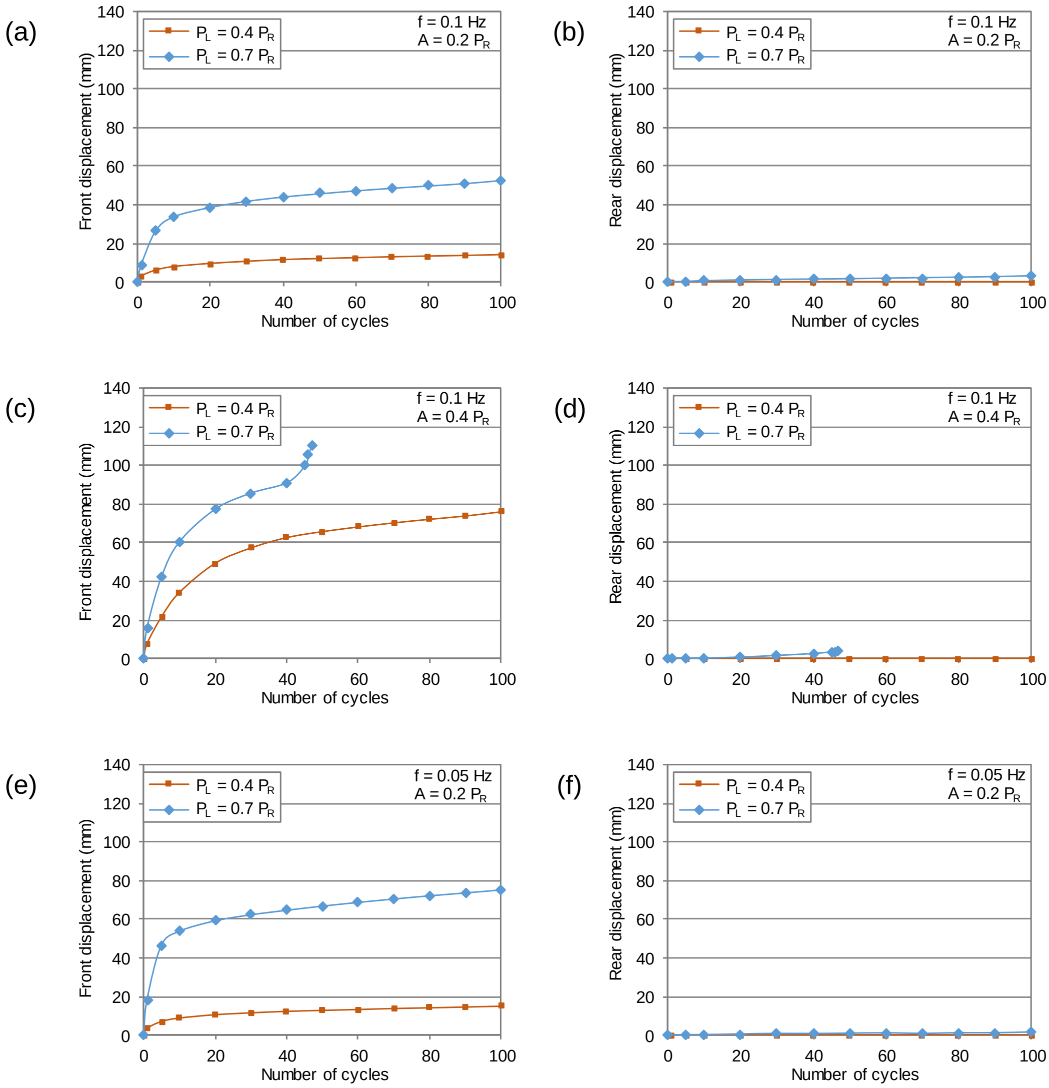

Fig. 7. Effect of P_L on the displacements accumulated at the GCR ends during cyclic loading: (a) front end (tests T1 and T5); (b) rear end (tests T1 and T5); (c) front end (tests T2 and T6); (d) rear end (tests T2 and T6); (e) front end (tests T3 and T7); (f) rear end (tests T3 and T7).

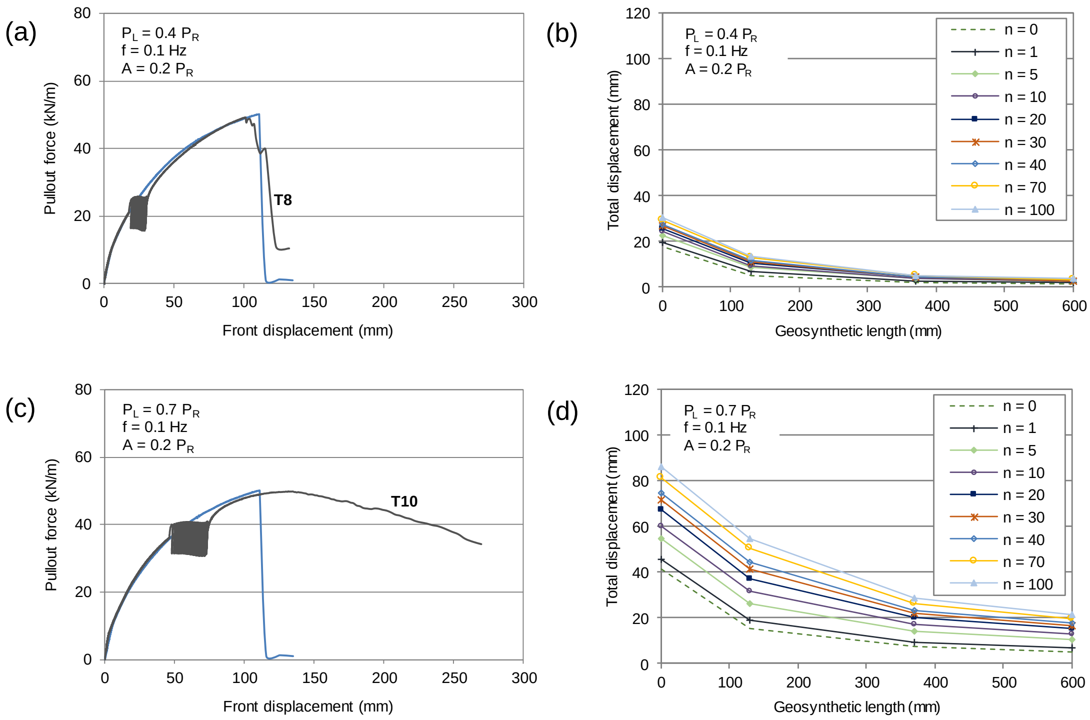

Fig. 8. Effect of P_L on the pullout behaviour of the GGR (f = 0.1 Hz, A = 0.2 P_R): (a) pullout force vs front displacement (P_L = 0.4 P_R); (b) total displacement over the GGR length (P_L = 0.4 P_R); (c) pullout force vs front displacement (P_L = 0.7 P_R); (d) total displacement over the GGR length (P_L = 0.7 P_R).

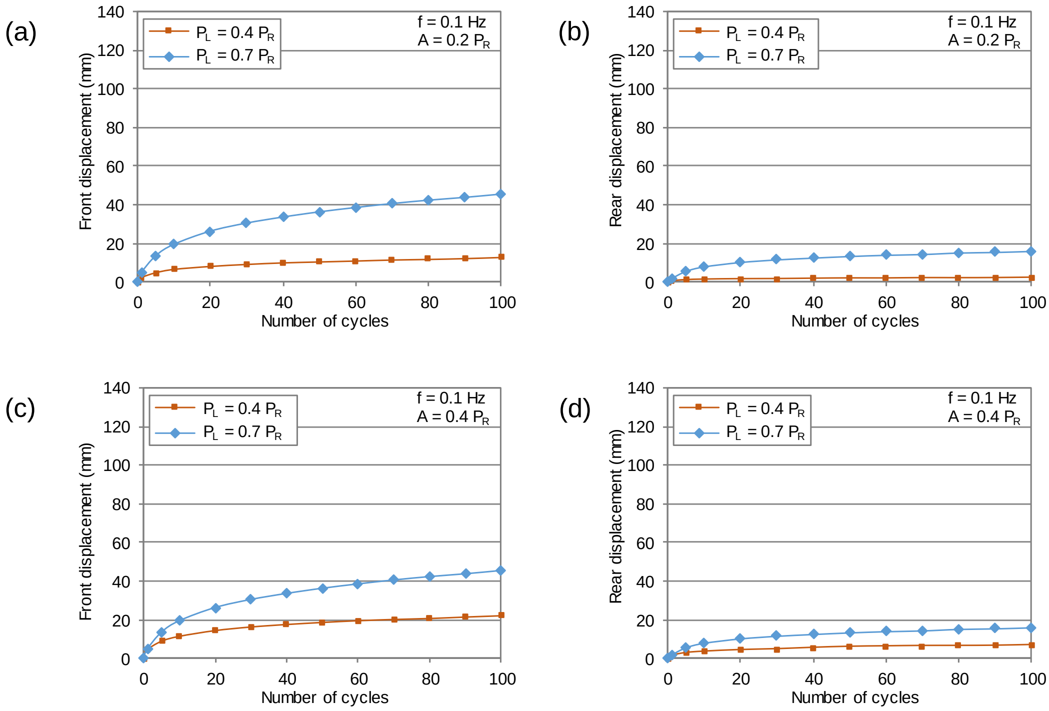

Fig. 9. Effect of P_L on the displacements accumulated at the GGR ends during cyclic loading: (a) front end (tests T8 and T10); (b) rear end (tests T8 and T10); (c) front end (tests T9 and T11); (d) rear end (tests T9 and T11).

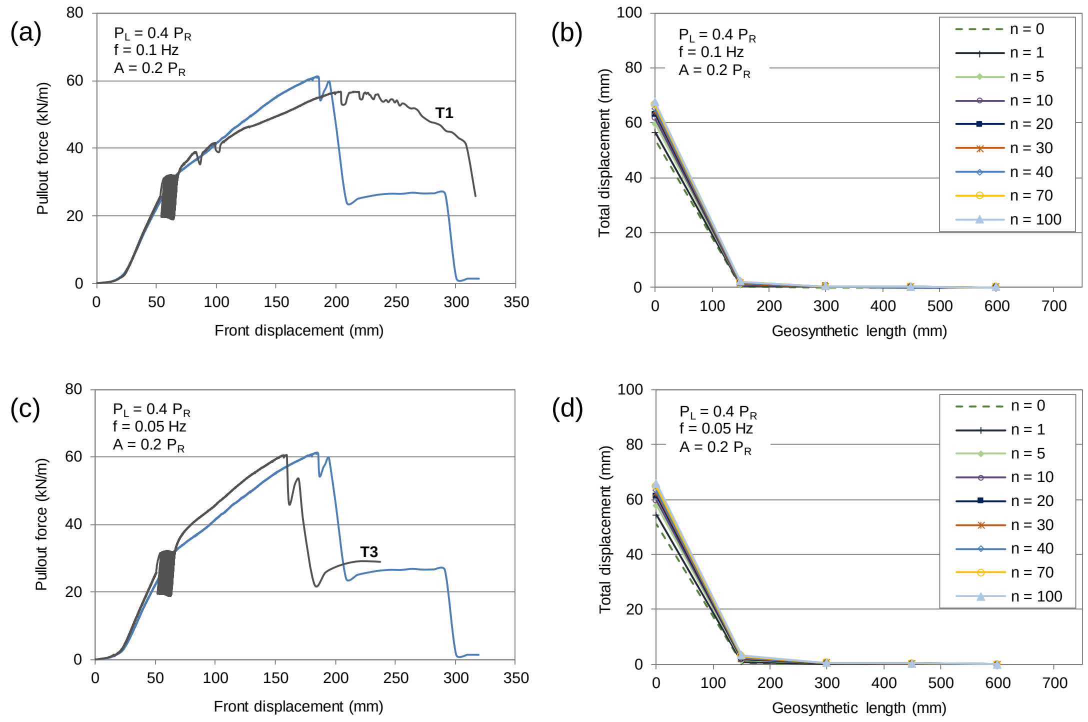

Fig. 10. Effect of frequency on the pullout behaviour of the GCR (P_L = 0.4 P_R, A = 0.2 P_R): (a) pullout force vs front displacement (f = 0.1 Hz); (b) total displacement over the GCR length (f = 0.1 Hz); (c) pullout force vs front displacement (f = 0.05 Hz); (d) total displacement over the GCR length (f = 0.05 Hz).

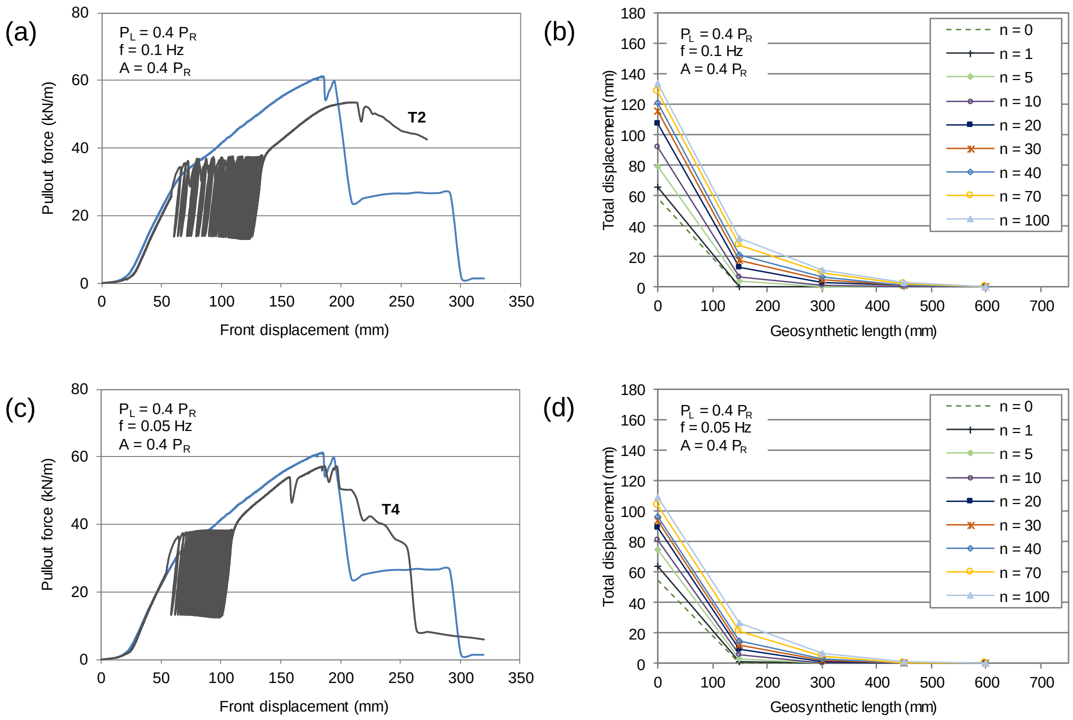

Fig. 11. Effect of frequency on the pullout behaviour of the GCR (P_L = 0.4 P_R, A = 0.4 P_R): (a) pullout force vs front displacement (f = 0.1 Hz); (b) total displacement over the GCR length (f = 0.1 Hz); (c) pullout force vs front displacement (f = 0.05 Hz); (d) total displacement over the GCR length (f = 0.05 Hz).

This manuscript is the accepted version of the paper:

Pullout behaviour of geosynthetics in a recycled construction and demolition material - Effects of cyclic loading, Transportation Geotechnics, Vol. 23, Article number 100346, https://doi.org/10.1016/j.trgeo.2020.100346

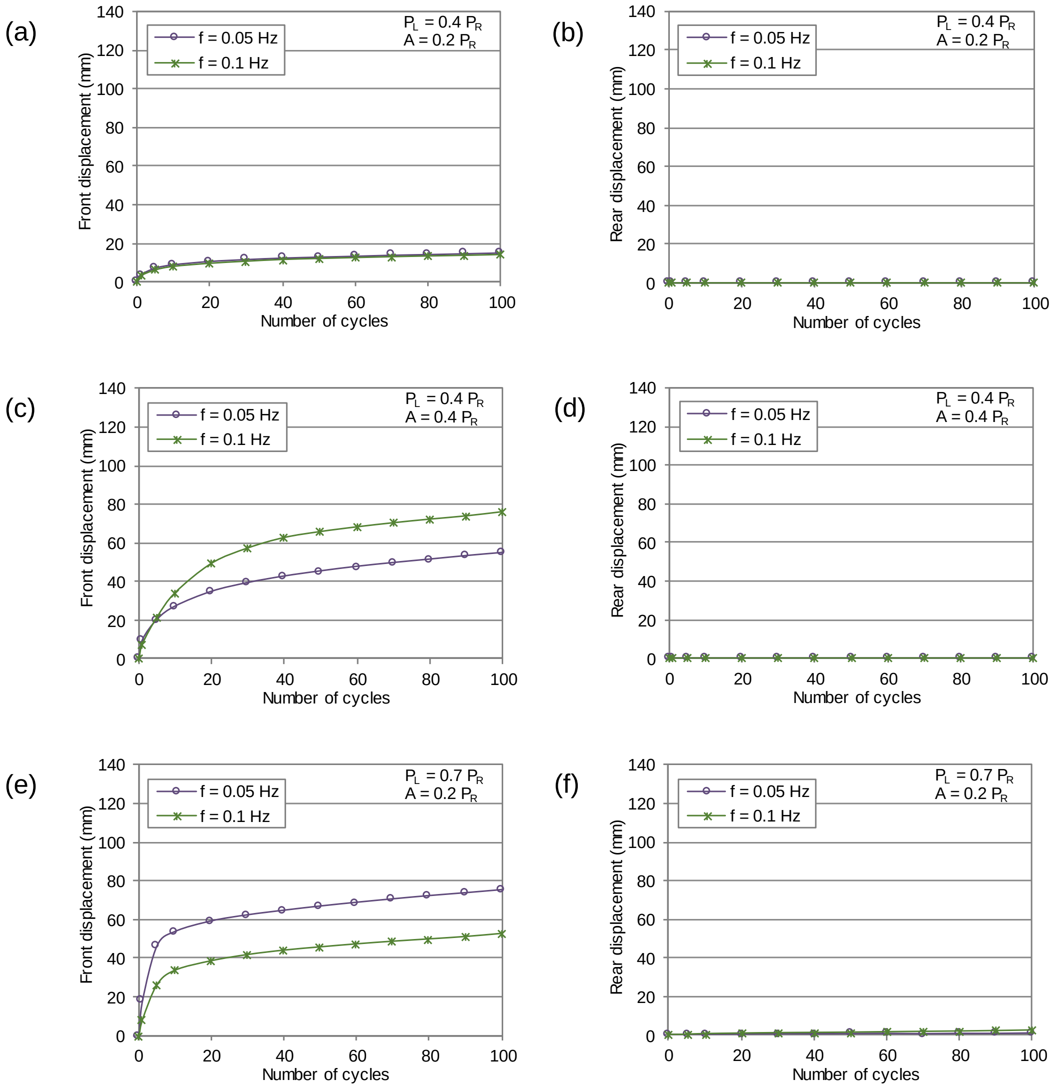

Fig. 12. Effect of frequency on the displacements accumulated at the GCR ends during cyclic loading: (a) front end (tests T1 and T3); (b) rear end (tests T1 and T3); (c) front end (tests T2 and T4); (d) rear end (tests T2 and T4); (e) front end (tests T5 and T7); (f) rear end (tests T5 and T7).

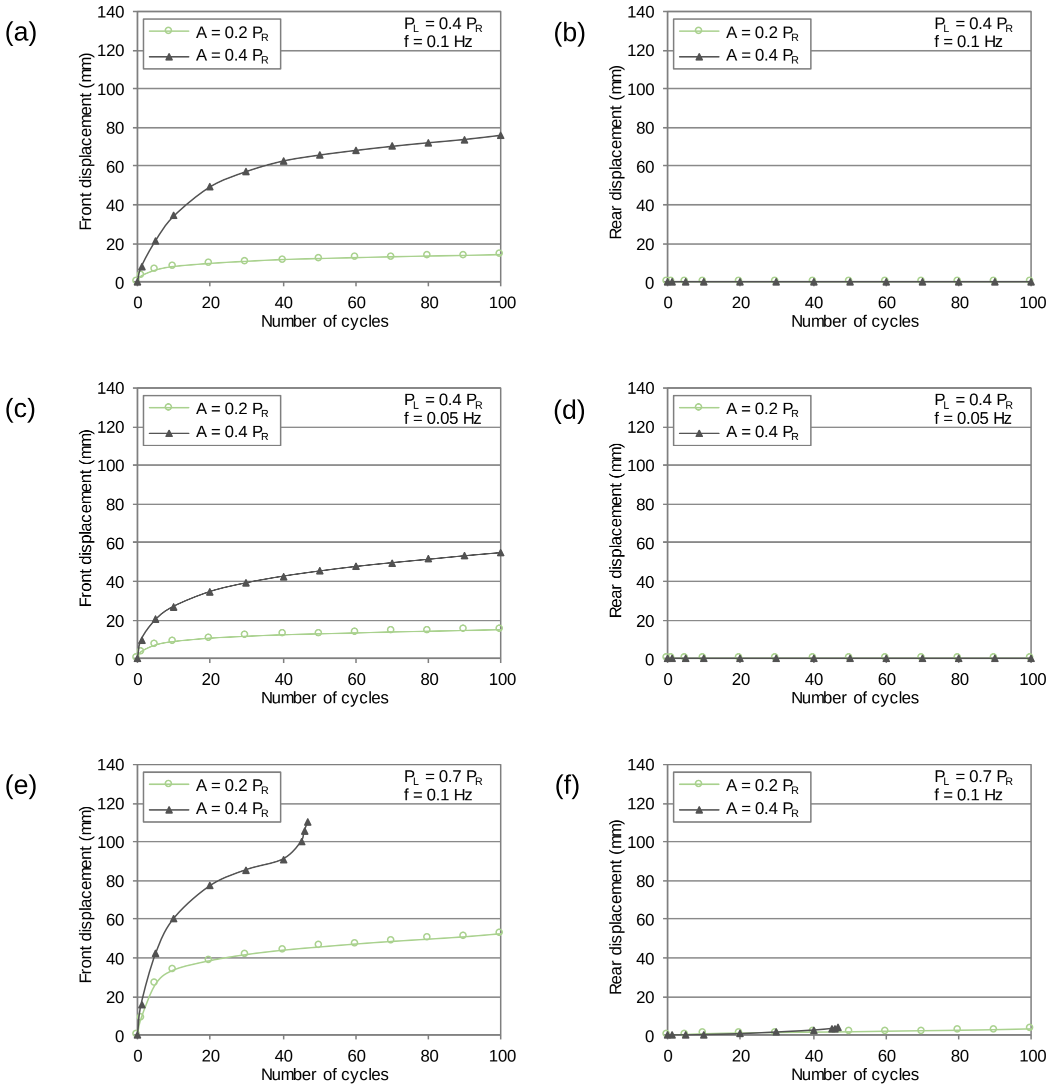

Fig. 13. Effect of amplitude on the displacements accumulated at the GCR ends during cyclic loading: (a) front end (tests T1 and T2); (b) rear end (tests T1 and T2); (c) front end (tests T3 and T4); (d) rear end (tests T3 and T4); (e) front end (tests T5 and T6); (f) rear end (tests T5 and T6).

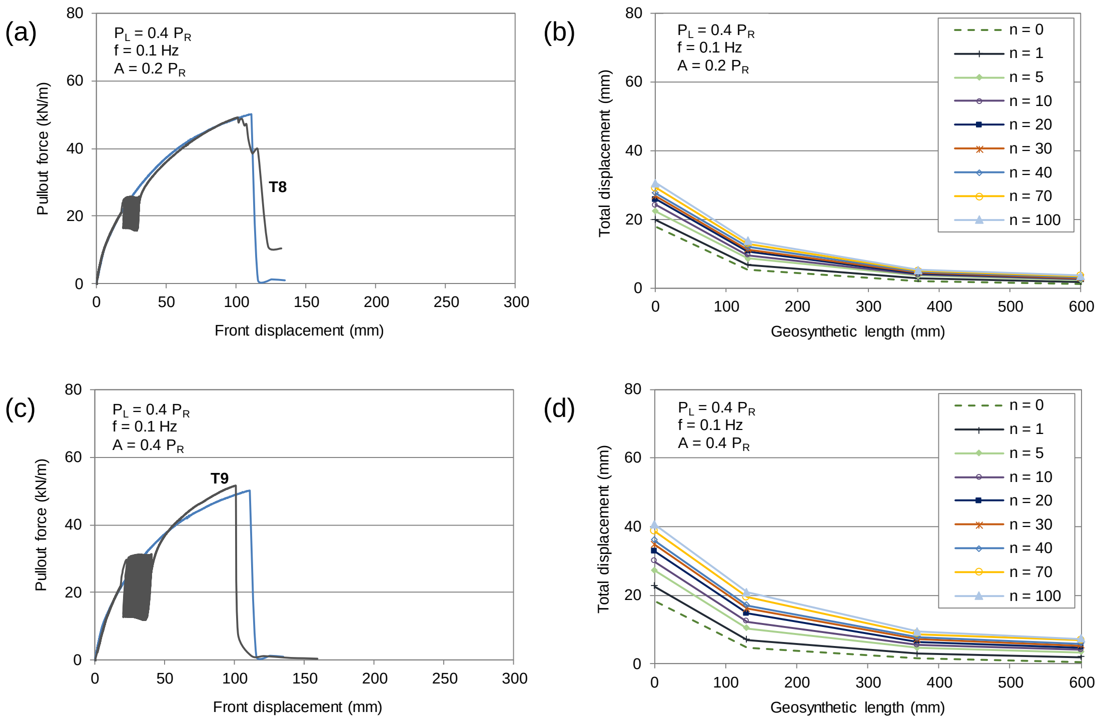

Fig. 14. Effect of amplitude on the pullout behaviour of the GGR (P_L = 0.4 P_R, f = 0.1 Hz): (a) pullout force vs front displacement (A = 0.2 P_R); (b) total displacement over the GGR length (A = 0.2 P_R); (c) pullout force vs front displacement (A = 0.4 P_R); (d) total displacement over the GGR length (A = 0.4 P_R).

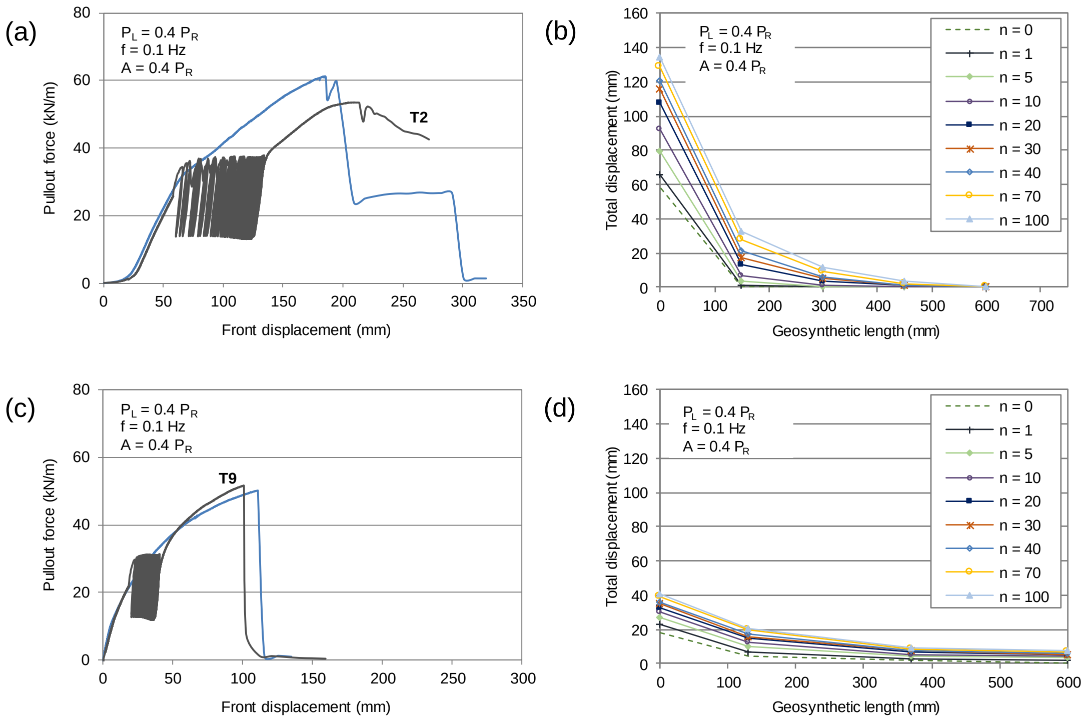

Fig. 15. Effect of geosynthetic type for $P_L = 0.4\ P_R$, f = 0.1 Hz and $A = 0.4\ P_R$: (a) pullout force vs front displacement of the GCR; (b) total displacement over the GCR length; (c) pullout force vs front displacement of the GGR; (d) total displacement over the GGR length.

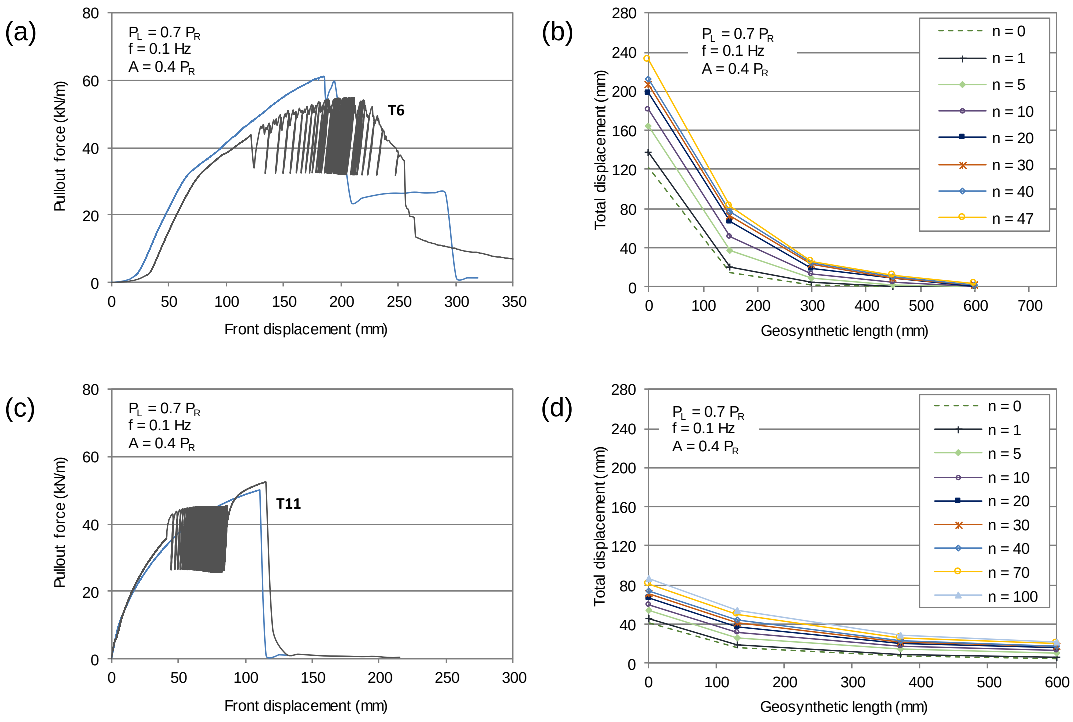

Fig. 16. Effect of geosynthetic type for P_L = 0.7 P_R, f = 0.1 Hz and A = 0.4 P_R: (a) pullout force vs front displacement of the GCR; (b) total displacement over the GCR length; (c) pullout force vs front displacement of the GGR; (d) total displacement over the GGR length.

This manuscript is the accepted version of the paper:

Pullout behaviour of geosynthetics in a recycled construction and demolition material - Effects of cyclic loading, Transportation Geotechnics, Vol. 23, Article number 100346, https://doi.org/10.1016/j.trgeo.2020.100346

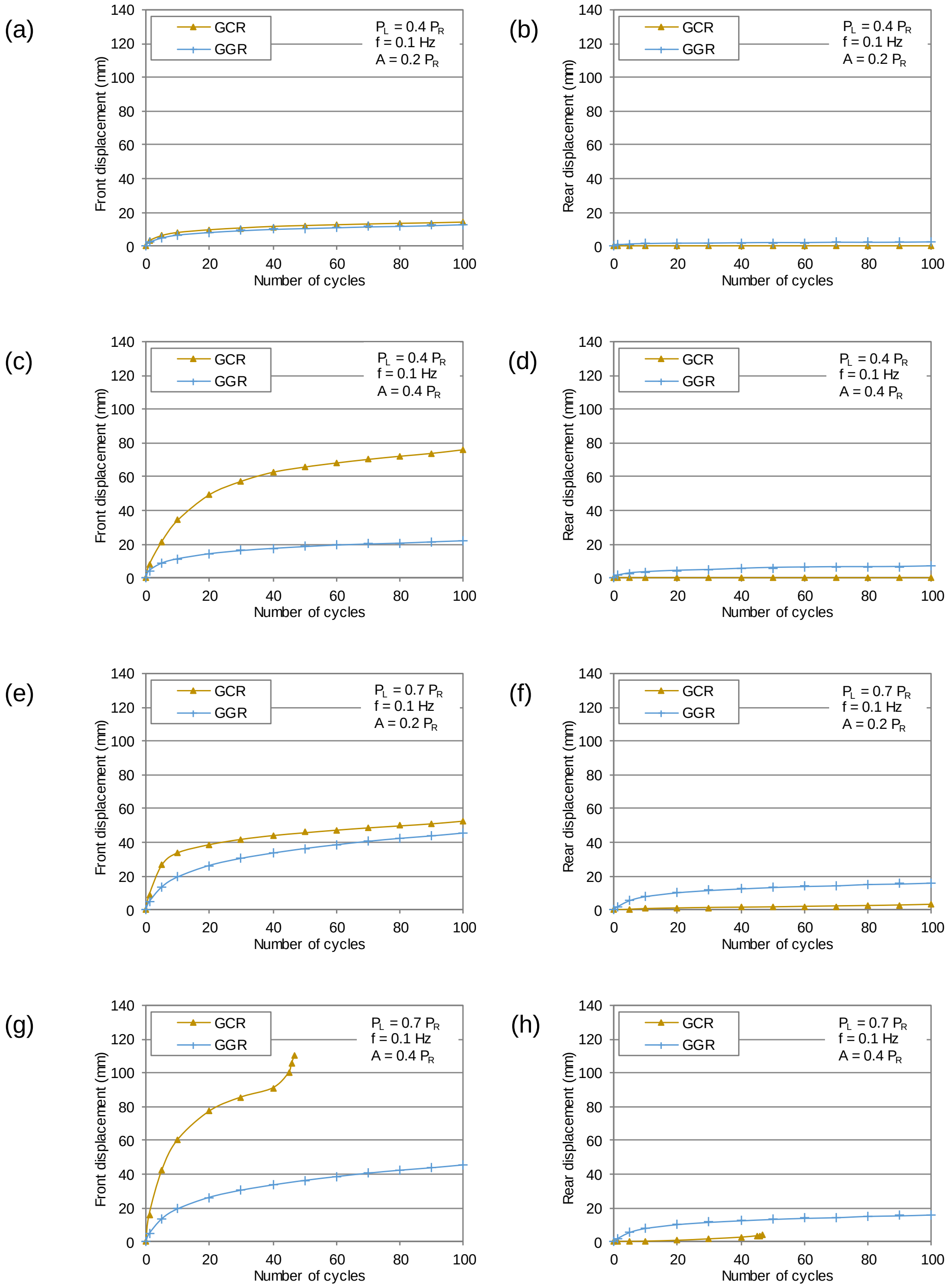

Fig. 17. Effect of geosynthetic type on the displacements accumulated at the reinforcement ends during cyclic loading: (a) front end (tests T1 and T8); (b) rear end (tests T1 and T8); (c) front end (tests T2 and T9); (d) rear end (tests T2 and T9); (e) front end (tests T5 and T10); (f) rear end (tests T5 and T10); (g) front end (tests T6 and T11); (h) rear end (tests T6 and T11).